International Journal of Heat and Mass Transfer 162 (2020) 120351

Contents lists available at ScienceDirect

International Journal of Heat and Mass Transfer

journal homepage: www.elsevier.com/locate/hmt

Machine learning algorithms to predict flow condensation heat transfer coefficient in mini/micro-channel utilizing universal data

Liwei Zhou[a,1], Deepak Garg[b,1], Yue Qiu[a], Sung-Min Kim[c], Issam Mudawar[d], Chirag R. Kharangate[a,*]

[a] Department of Mechanical and Aerospace Engineering, Case Western Reserve University, 10900 Euclid Avenue, Cleveland, OH, 44106, USA
[b] Mechanical and Aerospace Engineering Department, University of California, Los Angeles, CA, 90095, USA
[c] School of Mechanical Engineering, Sungkyunkwan University, 300 Cheoncheon-dong, Suwon, 16419, South Korea
[d] School of Mechanical Engineering, 585 Purdue Mall, West Lafayette, IN, 47907-2088, USA

ARTICLE INFO

Article history:
Received 23 May 2020
Revised 12 July 2020
Accepted 15 August 2020
Available online 4 September 2020

Keywords:
Machine learning
Neural networks
Gradient boosted trees
Condensation
Heat transfer

ABSTRACT

Miniature condensers utilizing mini/micro-channel has been recognized as one effective technique for designing a compact heat rejection device. However, because of the complex behaviors in phase-change systems like flow condensation, accurately predicting heat transfer coefficients can be a challenging task. In this study, a large database is utilized to develop machine-learning based models for predicting condensation heat transfer coefficients in mini/micro-channels. A consolidated database of 4,882 data points for flow condensation heat transfer in mini/micro-channels is amassed from 37 sources that includes 17 working fluid, reduced pressures of 0.039 – 0.916, hydraulic diameters of 0.424 mm – 6.52 mm, mass velocities of $50 < G < 1403$ kg/m^{2}s, liquid-only Reynolds numbers of 285 – 89,797, superficial vapor Reynolds number of 44 – 389,298, and flow qualities of 0 – 1. This consolidated database is utilized to develop four machine learning based models *viz.*, Artificial Neural Netoworks (ANN), Random Forest, AdaBoost and Extreme Gradient Boosting (XGBoost). A parametric optimization is conducted and ANN and XGBoost showed the best predicting accuracy. The models with dimensionless input parameters: *Bd, Co, Fr_f, Fr_{fo}, Fr_g, Fr_{go}, Ga, Ka, Pr_f, Pr_g, Re_f, Re_{fo}, Re_g, Re_{go}, Su_f, Su_g, Su_{fo}, Su_{go}, We_f, We_{fo}, We_g,* and *We_{go}* predicted the test data for ANN and XGBoost models with *MAEs* of 6.8% and 9.1%, respectively. The optimal machine-learning models performed better than a highly reliable generalized flow condensation correlation. Models were also able to predict excluded datasheets with reasonable accuracy when data points including the specific working fluid were part of the training dataset of the remaining datasheets. The work shows that machine learning algorithms can become a robust new predicting tool for condensation heat transfer coefficients in mini/micro channels.

1. Introduction

1.1. Flow condensation in mini/micro-channel

New technologies in automotive, consumer electronics, aerospace, and defense industries are in need of lightweight, highly efficient, and compact thermal management solutions. Two-phase flows including flow boiling in microchannel, spray and jet-impingement configurations has been shown to be a very effective cooling solution in such demanding environments [1–5]. The last few decades have seen unprecedented work in developing the heat acquisition components, while less importance has been given to the heat rejection components that also contribute significantly to the size and weight of the thermal management hardware. While commercial condensers can meet the cooling requirements, they are far too large and inefficient. Miniature condensers utilizing mini/micro-channel has been recognized as one effective technique for designing a compact heat rejection device.

Typical configurations in mini/micro-channel flow condensers include single or multi-channel in circular, square, or rectangular cross-sections and horizontal or vertical orientations with respect to Earth gravity. Flow condensation heat transfer in mini/micro-channels depends strongly on the flow pattern and flow transitions which impact the corresponding thermal behaviors observed in the channel. Flow patterns and flow transitions depend on many

* Corresponding author.
E-mail address: chirag.kharangate@case.edu (C.R. Kharangate).
[1] Contributed equally to this work.

https://doi.org/10.1016/j.ijheatmasstransfer.2020.120351
0017-9310/

Nomenclature

Bd	Bond number, $Bd = g(\rho_f - \rho_g)D_h^2/\sigma$
C	Confinement number
Co	Convection number, $Co = [(1-x)/x]^{0.8}(\rho_g/\rho_f)^{0.5}$
c_p	specific heat at constant pressure
c_v	specific heat at constant volume
D_h	hydraulic diameter of flow channel
E	total error
F	enhancement factor
E_m	loss function
Fr_f	saturated liquid Froude number, $Fr_f = [G(1-x)]^2/(\rho_f^2 g D_h)$
Fr_g	saturated vapor Froude number, $Fr_g = (Gx)^2/(\rho_g^2 g D_h)$
Fr_{fo}	liquid-only Froude number, $Fr_{fo} = G^2/(\rho_f^2 g D_h)$
Fr_{go}	vapor-only Froude number, $Fr_{go} = G^2/(\rho_g^2 g D_h)$
F_f	fluid-dependent parameter
f	activation function
G	mass velocity
Ga	Galileo number, $Ga = \rho_f g(\rho_f - \rho_g)D_h^3/\mu_f^2$
g	gravity acceleration
h	heat transfer coefficient
$h_{tp,exp}$	experiment measured condensation heat transfer coefficient
$h_{tp,pred}$	predicted condensation heat transfer coefficient
h_{fg}	latent heat of vaporization
i	connecting node i
j	connecting node j
k	liquid conductivity
Ka	Kapitza number, $Ka = \mu_f^4 g/\rho_f \sigma^3$
L	total number of input and output layers
l	layer
m	training example
M	number of training examples; molecular mass
MAE	mean absolute error
MSE	mean square error
n	number of input parameters
P	pressure
P_c	critical pressure
Pe_f	saturated liquid Peclet number, $Pe_f = Re_f\ Pr_f$
Pe_g	saturated vapor Peclet number, $Pe_g = Re_g\ Pr_g$
P_F	wetted perimeter of channel
P_H	heated perimeter of channel
P_R	reduced pressure, $P_R = P_c/P$
Pr_f	saturated liquid Prandtl number, $Pr_f = \mu_f c_{pf}/k_f$
Pr_g	saturated vapor Prandtl number, $Pr_g = \mu_g c_{pg}/k_g$
q''	heat flux
q''_H	heat flux based on heated perimeter of channel
R	relative roughness, $R = e/D_h$; Pearson's correlation coefficient
R^2	coefficient of determination
Re_f	saturated liquid Reynolds number, $Re_f = G(1-x)D_h/\mu_f$
Re_g	saturated vapor Reynolds number, $Re_g = GxD_h/\mu_g$
Re_{fo}	liquid-only Reynolds number, $Re_{fo} = GD_h/\mu_f$
Re_{go}	vapor-only Reynolds number, $Re_{go} = GD_h/\mu_g$
S	output, suppression factor
Su_f	saturated liquid Suratman number, $Su_f = \sigma\rho_f D_h/\mu_f^2$
Su_g	saturated vapor Suratman number, $Su_g = \sigma\rho_g D_h/\mu_g^2$
t	target value of training example
T	temperature
w	weight of connecting node
We_f	saturated liquid Weber number, $We_f = [G(1-x)]^2 D_h/(\rho_f\sigma)$
Weg	saturated vapor Weber number, $We_g = (Gx)^2 D_h/(\rho_g\sigma)$
Wefo	liquid-only Weber number, $We_{fo} = G^2 D_h/(\rho_f\sigma)$
Wego	vapor-only Weber number, $We_{go} = G^2 D_h/(\rho_g\sigma)$
We^*	modified Weber number
X	Lockhart-Martinelli parameter
x	quality, value of the node

Greek symbols

α	vapor void fraction
αr	regularization parameter
β	aspect ratio, exponential decay rate
δ	error at the node
ε	percentage data predicted within ±50%
θ	percentage data predicted within ±30%
μ	dynamic viscosity
ν	kinematic viscosity
λ	learning rate
ρ	density
σ	surface tension

Subscripts

c	critical
exp	experimental
f	saturated liquid, fluid
fo	liquid only
g	saturated vapor
go	vapor only
l	liquid
pred	predicted
tp	two phase; condensation
w	heated wall; inner wall
tt	turbulent liquid-turbulent vapor
tv	turbulent liquid-laminar vapor
vt	laminar liquid-turbulent vapor
vv	laminar liquid-laminar vapor

factors including orientation with respect to gravity, specific pressure, heat flux, flow rate, and channel geometry [6]. A study by Coleman and Garimella [7] conducted flow condensation experiments in multiple mini-channels with hydraulic diameters ranging from 2.67 mm to 4.91 mm, and showed existence of four flow regimes, namely annular, wavy, intermittent and dispersed. Each regime was in turn subdivided into multiple flow patterns as shown in Fig. 1(a). In another study, Kim et al. [8] conducted flow condensation experiments in micro-channels with hydraulic diameter of 1 mm, and showed existence of four flow regimes, namely annular, transition, slug and bubbly. Annular flow was further subdivided into smooth and wavy. These regimes and flow patterns are shown in Fig. 1(b). Considering such varying flow behaviors, dependent on both operating and geometric parameters, it is not easy to accurately predict flow condensation heat transfer coefficients in mini/micro channels.

1.2. Predicting heat transfer coefficient

Various approaches have been followed in literature to predicting heat transfer coefficient in mini/micro channel flow condensation systems. The most common and widely used approach is the development of empirical and semi-empirical correlations [9–17]. Researchers perform experiments over a range of geometric and flow parameters with select working fluids to develop correlations predicting heat transfer coefficients. While this approach gives ac-

curate heat transfer predictions for the configurations and tests under investigation, it should not be directly used to predict outside the tested range. Another approach that has also shown some success is the use of theoretical models based on the physical behavior of the flow. A good example is the annular flow condensation model by Kim and Mudawar [18]. This approach was developed for the annular flow regime, and therefore, its utilization is limited to this flow configuration. A more thorough control-volume-based approach involves computational fluid dynamics (CFD) simulations [19–22]. CFD approaches can predict transient flow and heat transfer behavior with detailed information on spatial and temporal distributions of void fraction, phase velocities and temperatures. However, due to limited model development efforts to date, their accuracy in predicting phase-change systems including flow condensation is limited [23]. Recent progress in high-performance computing has facilitated the employment of even more accurate Direct Numerical Simulation (DNS) that provide a direct solution of the Navier-Stokes equations [24]. These simulations are very computationally intensive and have not yet been successfully applied in microchannel condensation configurations.

An effective approach which relies on existing data from literature, is the use of generalized or universal correlations. With different researchers performing experiments on flow condensation heat transfer over the last few decades on numerous fluids and an extensive range of geometric and flow parameters, we now have reliable number of databases to develop these generalized correlations. A good generalized correlation developed for condensation in plain tubes is the study by Shah [25]. He amassed data from 39 sources that included 22 fluids for diameters ranging from 2 to 49 mm, and the correlation provided reasonably good predictions against the entire database, evidenced by an overall *MAE* of 14.4%. While the correlation by Shah [25] was for mini/macro-sized channels, Kim and Mudawar [26] developed a generalized correlation for mini/micro-channels. They amassed data from 28 sources that included 17 fluids for hydraulic diameters ranging from 0.424 to 6.22 mm, and the correlation provided reasonably good predictions against the entire database, evidenced by an overall *MAE* of 16.0%.

1.3. Machine learning models for thermal analysis

Conducting full-scale experiments or full CFD simulations of flow condensation requires enormous cost and time commitments. Heat transfer coefficient in flow condensation is usually a function of many independent properties, operating conditions, and dimensionless groups, each of them valid over a finite range of values. The generalized correlation approaches have shown how existing data from worldwide researches can be consolidated to develop high accuracy predicting tools [25,26]. The relationship between these parameters and their relevance to the output parameters can be deduced using novel machine learning based modeling techniques.

In the past few decades, unprecedented development of soft computing techniques, such as Artificial Neural Networks (ANNs), Decision Tree, Random Forest, Gradient Boosting, Adaptive Neuro-Fuzzy Inference Systems (ANFIS) and Support Vector Machines (SVM) have been performed, with their applications to a myriad of engineering problems. ANN are non-linear statistical models, like projection pursuit regression models, which extracts linear combination of derived features as inputs thereby modeling the target as non-linear function of these features [27]. Machine learning based modeling techniques for analyzing thermal systems have emerged as very promising in recent years with the highest interest seen in ANNs [28–36]. For heat transfer analysis, early work by Thibault *et al.* [37] showed that heat transfer data for practical problems can be correlated with ANNs. In another early study, Jambunathan *et al.* [38] showed that ANNs could model one-dimensional transient heat conduction for liquid crystal thermography and predict the convective heat transfer coefficients inside a duct. In recent years, we are seeing widespread implementation of ANN to more complex heat transfer problems. Naphon and Arisariyawong [39] and Naphon *et al.* [40] applied ANNs to analyze the heat transfer in a horizontal tube heat exchanger with spring insert and heat transfer in spirally fluted tubes, respectively, with predictions outperforming available correlations in literature. ANNs have also shown good performance in predicting heat transfer in nanofluid based flow systems [41–44]. In a recent study, Qiu et al. [45] consolidated saturated flow boiling heat transfer coefficient data from worldwide researchers and implemented ANNs with results showing the technique outperforming widely successful generalized correlation-based predicting tools. While ANNs are most common, recent studies have shown interest also moving toward other machine learning techniques. Baghban et al. [46] performed a comparison between artificial neural network, adaptive neuro-fuzzy inference system, and least squares support vector machine (LSSVM) models for predicting Nusselt numbers for helically coiled heat exchangers with water based carbon nanofluid. Their results showed LSSVM outperforming other techniques.

Even though machine learning methods have shown good predictions across many thermal system applications, they have not yet been applied to configurations like flow condensation. With available consolidated research on flow condensation in mini/microchannels, machine-learning methods can now be used to capture the relationship between relevant input parameters and condensation heat transfer coefficients.

1.4. Objective of study

A consolidated database consisting of 4,882 data points for flow condensation heat transfer in mini/micro-channels is amassed from 37 sources [47–83]. Table 1 provides key information on these individual databases incorporated into the consolidated database. The consolidated database includes a broad range of condensation heat transfer coefficient data points with the following coverage:

- Working fluids: R134a, R600a, R410a, R123, R245fa, R1234yf, R22, R12, R1234ze, R32, CO_2, FC72, Methane, R152a, Propane, R236fa, R404a
- Reduced pressures: $0.0396 < P_R < 0.92$
- Hydraulic diameter: $0.424\ \text{mm} < D_h < 6.52\ \text{mm}$
- Mass velocity: $50\ \text{kg/m}^2\text{s} < G < 1403\ \text{kg/m}^2\text{s}$
- Liquid-only Reynolds number: $285.28 \leq Re_{fo} = GD_h/\mu_f \leq 89{,}797$
- Superficial vapor Reynolds number: $44.43 \leq Re_g = GxD_h/\mu_g \leq 389{,}298$
- Flow quality: $0 < x < 1$

The objective of this study is to predict condensation heat transfer coefficient by using different machine learning models and compare their performance. In addition, the predicted results of the best models will be compared with the generalized condensation correlations to see how the machine learning technique compares with that predicting approach. Finally, the ability of models to predict completely excluded databases from the training set will also be verified to check the predicting capability of these tools.

2. Modeling

For this study, the codes are written in Python, and Pandas, Numpy and Scikit-learn [84] libraries are used to develop the machine learning algorithms. Specifically, four different machine learning based models for predicting condensation heat transfer coefficients in mini/micro-channels are developed and compared

Table 1
Condensation heat transfer database for mini/micro-channel flows included in the consolidated database.

Author(s)	Channel geometry*	Channel material	D_h [mm]	Fluid(s)	G[kg/m^{2}s]	Test mode^	Data points
Dobson *et al.* (1993a)	C single, H	copper	4.57	R134a, R12	75-653	quasi-local h $\Delta x = 0.1$-0.2	76
Dobson *et al.* (1993b)	C single, H	copper	4.57	R22	75-509	quasi-local h $\Delta x = 0.24$ (avg)	32
Dobson (1994)	C single, H	copper	3.14	R134a, R22	53-807	quasi-local h $\Delta x = 0.23$ (avg)	165
Hirofumi & Webb (1995)	C/R multi, H	aluminum	0.96 - 2.13	R134a	200-1403	quasi-local h $\Delta x = 0.12$ (avg)	62
Zhang (1998)	C single/multi, H	copper, aluminum	2.13, 3.25, 6.20	R134a, R22, R404A	200-1000	quasi-local h $\Delta x < 0.25$	80
Wang (1999)	R multi, H	aluminum	1.46	R134a	79-761	local h	748
Yan & Lin (1999)	C multi, H	copper	2.0	R134a	100-200	quasi-local h small Δx	78
Baird *et al.* (2003)	C single, H	copper	1.95	R123	170-570	local h	143
Kim *et al.* (2003)	R multi, H	aluminum	1.41	R410A, R22	200-600	quasi-local h $q'' = 0.5$ - 1.5 W/cm^2	19
Jang & Hrnjak (2004)	C single, H	copper	6.10	CO_2	197-406	quasi-local h small Δx	85
Cavallini *et al.* (2005)	R multi, H	aluminum	1.4	R410A, R134a	200-1400	quasi-local h $\Delta x = 0.2$-0.3	59
Mitra (2005)	C single, H	copper	6.22	R410A	200-800	quasi-local h $\Delta x = 0.21$ (avg)	144
Shin & Kim (2005)	C/R single, H	copper	0.493-1.067	R134a	100-600	quasi-local h small Δx	237
Andresen (2006)	C single/multi, H	aluminum, copper	0.76, 1.52, 3.05	R410A	200-800	quasi-local h $\Delta x = 0.32$ (avg)	315
Bandhauer *et al.* (2006)	C multi, H	aluminum	0.506, 0.761, 1.524	R134a	150-750	quasi-local h small Δx	128
Agra & Teke (2008)	C single, H	copper	4.0	R600a	57-118	quasi-local h small Δx	50
Kim *et al.* (2009)	C single, H	copper	3.48	CO_2	200-800	quasi-local h small Δx	48
Marak (2009)	C single, VU	stainless steel	1.0	methane	162-701	quasi-local h $\Delta x = 0.04$ (avg)	129
Matkovic *et al.* (2009)	C single, H	copper	0.96	R134a, R32	100-1200	local h	161
Park & Hrnjak (2009)	C multi, H	aluminum	0.89	CO2	200-800	quasi-local h $\Delta x < 0.3$	113
Agarwal *et al.* (2010)	R multi, H	aluminum	0.424, 0.762	R134a	150-750	quasi-local h small Δx	43
Bortolin (2010)	C/R single, H	copper	0.96, 1.23	R245fa, R134a	67-789	local h	309
Del Col *et al.* (2010)	C single, H	copper	0.96	R1234yf	200-1000	local h	66
Huang *et al.* (2010)	C single, H	copper	1.6, 4.18	R410A	200-600	quasi-local h $\Delta x = 0.2$	35
Ossama & Pradeep (2011)	C single, H	copper	6.52	CO2	50-200	local h smallΔx	89
Oh & Son (2011)	C single, H	copper	1.77	R22, R134a, R410A	450-1050	local h	108
Park *et al.* (2011)	R multi, VD	aluminum	1.45	R134a, R236fa, R1234ze(E)	100-260	local h	204
Derby *et al.* (2012)	R multi, H	copper	1.0	R134a	75-450	quasi-local h $\Delta x < 0.3$	140
Hossain *et al.* (2012)	C single, H	copper	4.35	R1234ze(E), R32 R410A	200-400	quasi-local h	91
Kim & Mudawar (2012)	R multi, H	copper	1.0	FC-72	118-367	local h	268
Kittipong et al (2013)	R multi, H	aluminum	1.11,1.2	R134a	350-690	local h $\Delta x = 0.08$	61
Na Liu et al (2013)	C/R single, H	stainless steel	1.152, 0.952	R152a	200-800	local h	78
Heo *et al.* (2013)	R multi, H	aluminum	1.5	CO2	400-1000	local h $\Delta x = 0.06$	95

(*continued on next page*)

Table 1 (*continued*)

Gomez *et al.* (2014)	R multi, H	aluminum	1.16	R1234yf,	350-945	local h Δx=*0.022-0.125*	192
Goohyun & Jaeseon (2016)	C single, H	copper	7.75	R245fa	150-700	quasi-local *h* smallΔx	21
Jatuporn Kaew-On et al (2016)	C single, H	copper	3.51	R134a	380-750	local h	60
Liu *et al.* (2016)	C/R single H	stainless steel	1.085, 0.952	propane, R1234ze(E), R22	200-800	local h Δx=*0.032-0.074*	150
Total							4882

* C: circular, R: rectangular, H: horizontal, VU: vertical upward, VD: vertical downward; ^quasi-local: heat transfer coefficient averaged over the flow channel

in this study: Artificial Neural Network, Random Forest, Adaptive Boosting, and Extreme Gradient Boosted Trees.

The usual way of splitting the data between training and test datasets is 70%–30%, 75%–25%, or 80%–20%. A good rule of thumb is to have the training dataset be 3–4 times more than the test dataset as the bulk of the model performance depends on training dataset volume. Data partitioning is investigated by utilizing different combinations of test and train data and 75%–25% split ratio is seen to be acceptable. Therefore, the consolidated dataset was split into training and test datasets with 75%–25% split ratio with 3662 training data points and 1220 test data points. The accuracy of the models is ascertained mainly using mean absolute error (*MAE*), which is defined as

$$MAE = \frac{1}{N}\sum \frac{\left|h_{\mathrm{tp,pred}} - h_{tp,exp}\right|}{h_{tp,exp}} \times 100\% \tag{1}$$

Many studies with machine learning algorithms use *R*-squared error (coefficient of determination or R^2) which will also be used for understanding model predictability. R^2 statistic that is close to 1 indicates that a large proportion of the variability in the target variable has been explained by the model. R^2 is defined as

$$R^2 = 1 - \frac{\sum\left(h_{\mathrm{tp,exp}} - h_{tp,pred}\right)^2}{\sum\left(h_{\mathrm{tp,exp}} - \bar{h}_{tp,\mathrm{exp}}\right)^2} \tag{2}$$

In addition, the adjusted R^2 that is an attempt to account for the phenomenon of spurious increase in R^2 value when additional predictors are added to the model, will also be used for understanding model predictability. It is defined as

$${R_{adj}}^2 = 1 - \left(1 - R^2\right)\left[\frac{n-1}{n-p-1}\right] \tag{3}$$

2.1. Artificial neural networks (ANN)

The first model that is being developed is an artificial neural network model. Neural networks are frameworks for representing non-linear functional mappings between a set of input variables and a set of output variables. The representation of non-linear functions of several variables in terms of compositions of non-linear functions of a single variable is achieved using activation functions [85]. Generally, these models are considered as black boxes that are unable to provide any insight about the system features and also have unknown parameters known as “weights” [86]. These weights are associated with the links between the nodes (neurons) of the adjacent layers. A set of input parameters are fed into the network and with the condition that there are no feedback loops, the output parameters can be calculated explicitly using input parameters and weights. Fig. 2(a) shows such a feed forward neural network with input layer and output layer. The units not belonging to input and output are collectively called as hidden layers.

To fit a neural network model, the values of the weights needs to be estimated using the training data. Regression and classification are two broad types of supervised learning techniques. In a regression problem, the sum of squared errors is used as the measure of fit, while in classification problems, cross-entropy (deviance) is used. Weights of the neural network are estimated by back-propagation algorithm, which is also called as the delta rule or a two pass algorithm [87]. In the forward pass, the output is calculated using the current value of the weights and the error estimated in back-propagated backwards in the second pass. Due to the compositional form of the model, gradient of the weight is conveniently derived using the chain rule of differentiation. In order to prevent overfitting, some regularization is needed through a penalty term or doing that indirectly by early stopping [27].

2.2. Tree-based models

Three different tree-based models derived from decision trees are investigated in this study: Random Forest, Adaptive Boosting, and Gradient Boosting. A simple decision tree suffers from the problem of high variance, i.e. if the training data is split into multiple parts then the results obtained from each one of the splits can be quite different [88]. To sort this issue, Random Forest method aggregates a number of decision trees and works on the principle of “bootstrap aggregation” (bagging), to reduce the variance of the machine learning model. In bagging, each training set is formed by constructing a bootstrap replication of the original training set [89]. On the other hand, Boosting is a process in which the trees are grown sequentially, using information from previously constructed trees. AdaBoost and gradient boosting models are based on this principle of fitting the trees iteratively on residuals rather than the target variable.

2.2.1. Adaptive boosting (AdaBoost)

The second model that is being developed is the adaptive boosting model (AdaBoost). AdaBoost was the first boosting algorithm proposed by Freund and Schapire [90] and remains one of the most widely used and studied algorithms with numerous applications. A simple illustration of the principle of AdaBoost is shown in Fig. 2(b). Here, we explain how the AdaBoost model performs a simplified two-dimensional classification of squares and circles. In the first step, a decision stump (D1), a one level decision tree, generates a vertical classification boundary that classifies circles on the left side and squares on the right side. However, this elementary model incorrectly classifies the three circles on the right side also as squares. Further, in the next iteration, the model will place higher weights on the errors made on the previous iteration (D1). Here, a horizontal classification boundary generated by the second decision stump (D2) classifies the remaining three circles. However, even this model incorrectly classifies one square as a circle. To correct, this, in the next iteration, the weight of the misclassified square is increased further and the third decision stump

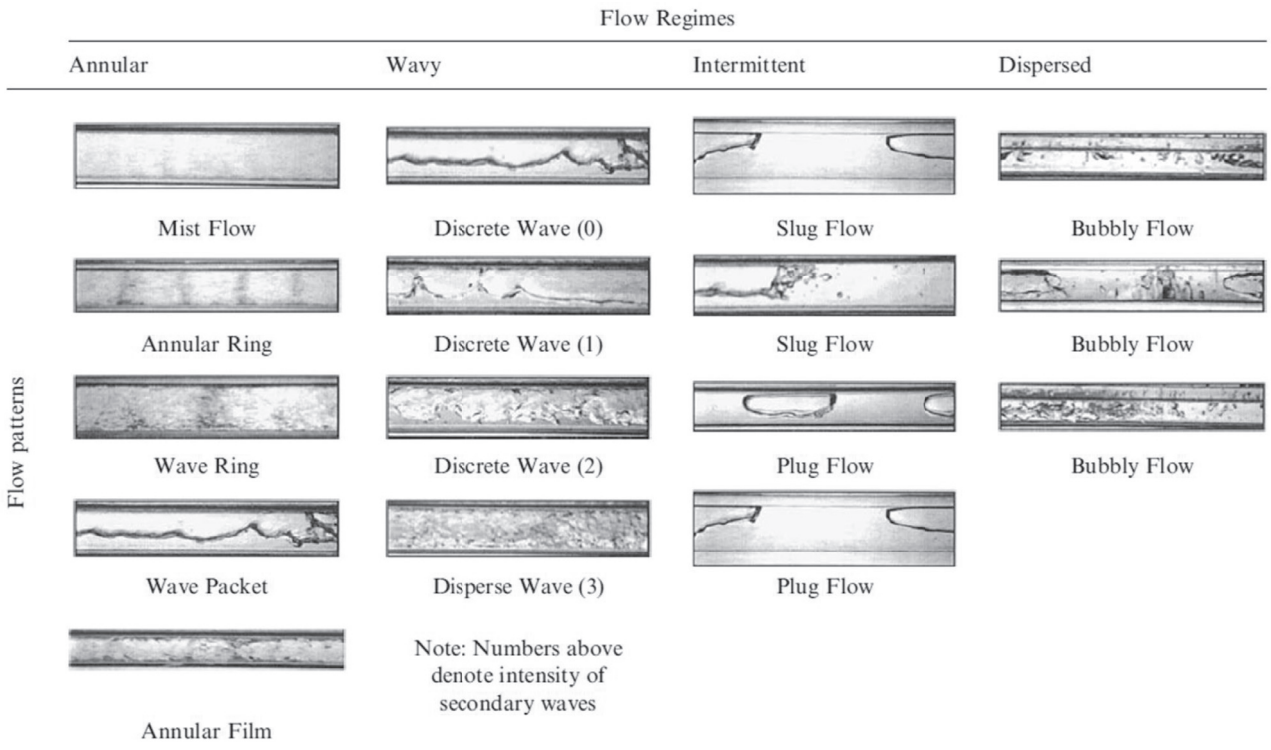

(a)

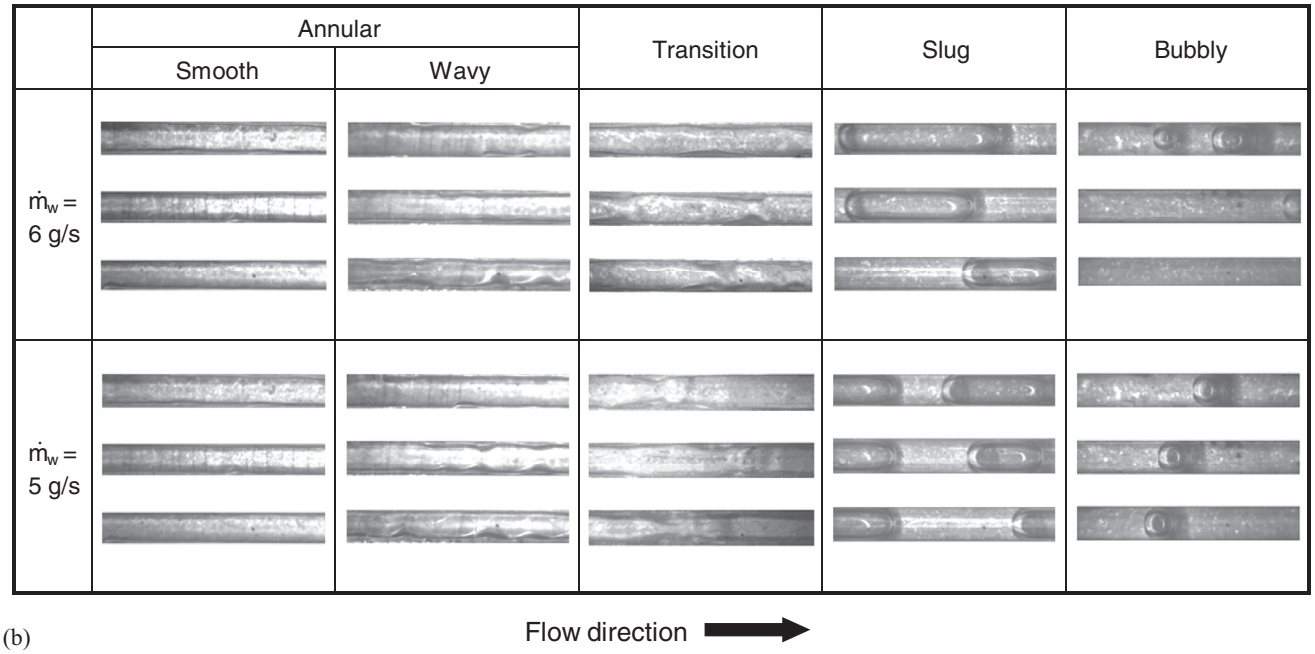

(b)

Fig. 1. (a) Representative photographs of R-134a condensation flow regimes in channels of hydraulic diameter between 2.67 – 4.19 mm (Adapted from Coleman and Garimella [7]). (b) Representative photographs of FC-72 condensation flow regimes in a flow channel of hydraulic diameter of 1 mm (Adapted from Kim *et al.* [8]).

D3 is successful in separating that square from the circle. Hence, the final boosted model is the combination of all the three decision stumps (D1, D2 and D3) and is better than any of the three individual models.

The Adaboost algorithm is mathematically explained as follows and shown in Table 2 [91]. Consider m label training examples (x_1,y_1), (x_2,y_2), ……., and (x_m,y_m). The x_i's are is some domain χ while $y_i \in \{-1,1\}$. The classifier $\hat{f}(x)$ can take one of the values from {-1,1}. The Adaboost algorithm generates a sequence of weak classifiers induced on a distribution of weights over the training set. A single-split classification tree with only two terminal nodes is one such weak classifier. The algorithm is initialized with all the weights initially set to zero, but during each iteration, the training example that was misclassified on the previous iteration gets

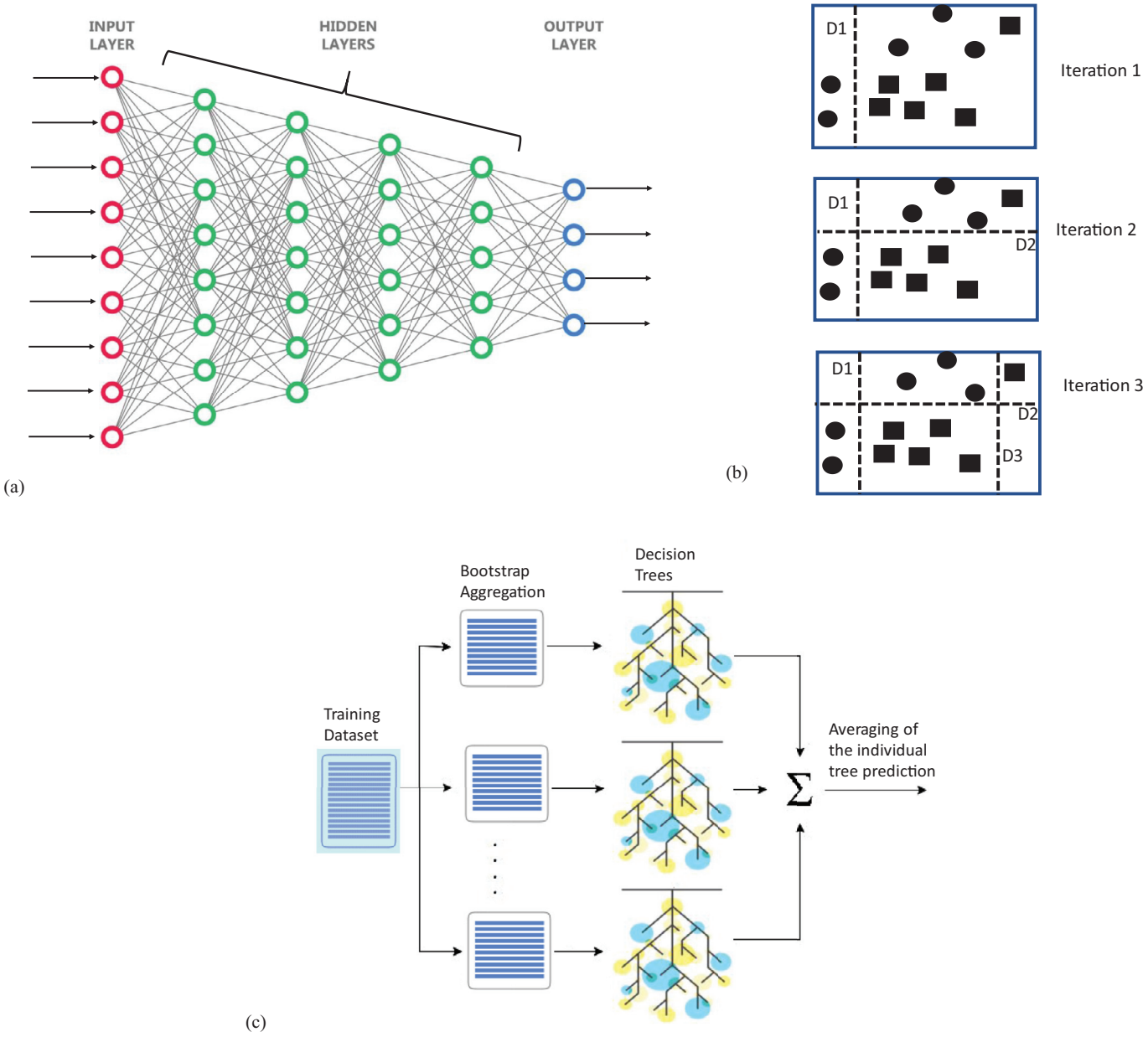

Fig. 2. (a) A feed forward neural network model. (b) AdaBoost model-based simplified 2-dimensional classification. (c) Random forest model architecture.

Table 2
Machine learning model algorithms (Adapted from [91]).

	Procedures	Output
Adaptive Boosting	1. Initialize observation weights $\omega_i = \frac{1}{M}$ 2. **For** t=1 to T **do** 3. Fit$f_t(x)$as the weak classifier on the training data usingω_i 4. Compute the weighted error rate as $err_t = \frac{\sum_{i=1}^{m} \omega_i \cdot I(y_i \neq f_t(x_i))}{\sum_{i=1}^{m} \omega_i}$ 5. Let$\alpha_t = \log((1 - err_t)/err_t)$ 6. Update$\omega_i \leftarrow \omega_i \cdot \exp[\alpha_t \cdot I(y_i \neq f_t(x_i))]$scaled to sum to one $\forall i \in \{1, ..., M\}$ 7.**end for**	$\widehat{f}(x) =$ $sign[\sum_{t=1}^{T} \alpha_t \cdot \widehat{f}_t(x)]$
Gradient Boosting	1. Initialize $f_0(x)$ to be a constant, $f_0(x) = \arg\min_{\beta} \sum_{i=1}^{M} L(y_i, \beta)$ 2. **For** t=1 to T **do** 3. Compute the negative gradient as the working response $r_i = -[\frac{\partial L(y_i, f(x_i))}{\partial f(x_i)}]_{f(x)=f_{t-1}(x)}, i = \{1, ...M\}$ 4. Fit a regression model to r_i by least-squares using the input x_i and get the estimate a_t of $\beta h(x; a)$ 5. Get the estimate β_t by minimizing $L(y_i, f_{t-1}(x_i) + \beta_t h(x_i; a_t))$ 6. Update $f_t(x) = f_{t-1}(x) + \beta_t h(x; a_t)$ **end for**	$\widehat{f}(x) = f_T(x)$

more weight on the next one. Thus, with each successive iteration the algorithm is forced to focus on examples which are difficult to learn. The final classifier is the weighted majority vote of the individual classifiers. It has to be noted that boosting risks overfitting which can be remedied by regularization and stochastic gradient boosting methods [92].

2.2.2. Random forest

The third model that is being developed is the random forest model which works on the law of large numbers, and hence, does not have an overfitting issue. Random forest is an ensemble learning methodology first proposed by Breiman [93], in which the performance of a number of weak learners is boosted via a voting scheme as shown in Fig. 2(c). Random forest adds an additional layer of randomness to bagging. In addition to constructing each tree using bootstrap sampling (i.e. randomly sampling with replacement) of the data, random forest change how the classification or regression trees are constructed. Each node in random forest is split using a subset of predictors randomly chosen at that node. The samples not selected are known as out-of-bag (OOB) samples [36]. The bootstrapping procedure leads to better model prediction as it decreases the variance of the model without increasing its bias. Each tree is trained on a slightly different dataset, and therefore, are de-correlated from each other.

2.2.3. Extreme gradient boosting (XGBoost)

The final model that is being developed is the gradient boosting model. This model was first introduced by Friedman [94] and is a manifestation of the gradient descent algorithm in function space (prediction space). Gradient boosting algorithms optimize cost function over the function space by iteratively choosing a weak hypothesis pointing in the negative gradient direction. The gradient boosting algorithm uses a two-step procedure as shown in Table 2 [91]. The first step estimates α_t, which represents the split variable, their split values and the fitted values at each terminal node of the tree. By fitting a weak learner to the negative gradient of the loss function using least squares. A variant of the gradient boosting model, is the extreme gradient boosting [95], which will be utilized in this study. XGBoost can be interpreted as a Newton method in function space and offers the possibility of penalizing the complexity of the trees [96].

2.3. Parametric optimization

For the ANN model, parametric optimization was done using the manual search technique. Optimization of neural network is not straightforward as it depends on several aspects like number of independent variables available, amount of noise in the data, activation function used, loss function and the total data available. Table 3 shows the different ANN model parameters that are optimized heuristically (manual search) and proposed to be used through this study. The important parameters include the learning rate, λ, and L2 regularization parameter (α_r) which are set to 0.001. In addition, the exponential decay rate of the first and second moments is specified to be 0.9 and 0.999, respectively. The loss function to minimize is the mean squared error (*MSE)* loss, as it is the preferred loss function under the inference framework of maximum likelihood [97]. The Adam optimization algorithm [99] is run until the *MSE* loss is minimized with maximum number of iterations without satisfying the tolerance criterion of 0.001 is set to 100. In addition, it is necessary to evaluate the number of hidden layers and number of units in each layer. The number of nodes in each layer is selected heuristically as there is no rule of thumb that dictates the network width and depth. Usually, the number of layers in the first input layer is more, and then we select the network architecture that tapers down as we have only one output parameter. For a fixed number of input parameters as shown in Table 4, different combinations of hidden layers are investigated. For models with few hidden layers like (10) and (20,10), the *MAE*s are 19.9% and 17.9%, respectively. The corresponding R^2s are 0.82 and 0.85, respectively. With more hidden layers, models with (50,40,30,20,10) and (70,60,50,40,30,20,10) show *MAE*s of 9.7% and 8.9%, respectively. The model with a large hidden layers network with (150,140,130,120,110,100,90,80,70,60,50,40,30,20,10) reached the best performance with an *MAE* of 6.8%, R^2 of 0.98, and adjusted R^2 of 0.98. Further increase in hidden layer does not improve the performance and can lead to overfitting with higher *MAE* in the test dataset. Finally, the hidden layers network of (150,140,130,120,110,100,90,80,70,60,50,40,30,20,10) was selected as the final model for the ANN network analysis performed in this investigation.

Hyperparameter tuning was utilized to perform parametric optimization for the three tree based models. Hyperparameters are model specific properties that are fixed even before the model is trained and tested on the data. Hyperparameter tuning is searching for the most optimal sets of parameters for the model. This was achieved using the grid search technique where all possible combination of predefined hyperparameter value range are tested to select the parameters resulting in the best model performance. Table 3 shows the hyperparameter for the Adaboost model. The loss function used for optimization is the exponential loss function. The base estimator is a decision tree with depth of three while the limit for the maximum number of base estimators at which the boosting is terminated is 100. While there is a trade-off between learning rate and estimators, the learning is set to 0.1. Table 3 also shows the optimal hyperparameters for the Random Forest. The numbers of trees in the forest is capped at 50 with the maximum depth of the trees being 6. The function to measure the criterion of the split while creating decision tree is mean square error, which is similar to the variance reduction method. Lastly, Table 3 also shows the optimal parameters used for XGBoost model. Since, XGBoost is prone to overfit [95], only the parameter to control it are discussed in the text and all others are shown in Table 3. The step size value during update, η, is proposed to be 0.3, which is used to prevent overfitting. The maximum depth of the tree is set as 3 because increasing this value also makes the model more likely to overfit. The regularization parameters α (L1) and λ (L2) are taken to be 0 and 1, respectively. A detailed discussion on different search techniques as utilized by us for optimizing machine learning models is provided in Bergstra *et al.* [98,99] and will not be discussed further in this study.

3. Results and discussion

3.1. Model performance comparison

The consolidated data for condensation in mini/micro-channels that is amassed in this study is utilized to test, develop, and compare the predicting performances for the four machine learning models under investigation. A combination of input parameters, including flow parameters, geometric parameters, fluid properties and relevant dimensionless numbers, is utilized to setup the model with the heat transfer coefficient being the only output parameter. These parameter selections are made such that we can maintain model scalability in the future without any redundancies.

First, we understand the impact of selecting specific combinations of input parameters on ANN model's heat transfer coefficient predicting capability. Table 5 compares the predicting performance for the ANN model based on different combinations of input parameters. Selecting models with low input parameters like those shown with inputs *Bd, Pr_f, Re_f,*and Fr_f (Case 1) and D_h, *G, x*

Table 3
Optimized model parameters.

Model	Parameter	Value
ANN	Activation function	ReLu
	L2 Regularization Parameter, α	0.001
	Solver	Adam
	Batch Size	200
	Learning rate, λ	0.001
	Exponential decay rate for estimates of first moment vector, $\beta 1$	0.9
	Exponential decay rate for estimates of second moment vector, $\beta 2$	0.999
	Tolerance	0.001
	Hidden Layers	(150,140,130,120,110,100,90,80,70,60,50,40,30,20,10)*
AdaBoost	Base estimator	Decision Tree (Depth = 3)
	Number of estimators	100
	Learning rate	0.1
	Loss	Exponential
Random	Number of estimators	50
Forest	Max depth	6
	Max features	Number of features
	Bootstrap	Yes
	Max samples	Training data size
	Loss	Mean square error
XGBoost	η	0.3
	Υ	0.0
	Max depth	3
	Minimum child weight	1
	Maximum delta step	0
	Subsample	1
	Sampling Method	Uniform
	λ	1
	α	0
	Scale Pos Weight	1
	Refresh Leaf	1
	Grow Policy	Depthwise
	Max Leaves	0
	Max Bin	256

* Based on optimization conducted in Table 4

Table 4
ANN model predictions for fixed input parameters and different combinations of hidden layers.

Test Case	ANN Model Hidden Layers	Input Parameters	MAE	R^2	Adjusted R^2
0	(180,170,160,150,140,130,120,110,100,90,80,70,60,50,40,30,20,10)	Bd, Co, Fr_f, Fr_{fo}, Fr_g,	7.38	0.98	0.98
1	(170,160,150,140,130,120,110,100,90,80,70,60,50,40,30,20,10)	Fr_{go}, Ga, Ka, Pr_f,	7.13	0.97	0.97
2	(160,150,140,130,120,110,100,90,80,70,60,50,40,30,20,10)	Pr_g, Re_f, Re_{fo}, Re_g,	7.14	0.98	0.98
3	**(150,140,130,120,110,100,90,80,70,60,50,40,30,20,10)***	Re_{go}, Su_f, Su_g, Su_{fo},	6.80	0.98	0.98
4	(140,130,120,110,100,90,80,70,60,50,40,30,20,10)	Su_{go}, We_f, We_{fo},	7.34	0.98	0.98
5	(130,120,110,100,90,80,70,60,50,40,30,20,10)	We_g, We_{go}	7.56	0.97	0.97
6	(120,110,100,90,80,70,60,50,40,30,20,10)		8.29	0.97	0.97
7	(110,100,90,80,70,60,50,40,30,20,10)		9.47	0.97	0.97
8	(90,80,70,60,50,40,30,20,10)		8.64	0.97	0.97
9	(70,60,50,40,30,20,10)		8.86	0.97	0.97
10	(50,40,30,20,10)		9.70	0.96	0.96
11	(20,10)		13.12	0.93	0.93
12	(20)		17.88	0.85	0.84
13	(10)		19.88	0.82	0.82

*Final selected ANN model configuration

Table 5
Model predictions for different combinations of input parameters.

Case	Parameters	Models	*MAE*	R^2	*Adjusted* R^2
1	Bd, Pr_f, Re_f, Fr_f	ANN	40.69	0.36	0.35
		Random Forest	42.09	0.48	0.47
		AdaBoost	56.25	0.34	0.33
		XGBoost	38.23	0.50	0.50
2	D_h, G, x	ANN	14.89	0.85	0.85
		Random Forest	23.85	0.73	0.73
		AdaBoost	40.14	0.59	0.59
		XGBoost	13.48	0.89	0.89
3	c_{pf}, c_{pg}, P_c, c_{vf}, c_{vg}, ρ_f, ρ_g, P_F, P_H, P_R,P,β, D_h,h_{fg},k_f, k_g, G, x, T, μ_f, μ_g, σ	ANN	6.17	0.99	0.99
		Random Forest	21.52	0.86	0.86
		AdaBoost	41.49	0.68	0.68
		XGBoost	7.34	0.98	0.98
4	Bd, Co, c_{pf}, c_{pg}, P_c, c_{vf}, c_{vg}, ρ_f, ρ_g, Fr_f, Fr_{fo}, Fr_g, Fr_{go},Ga, Ka, P_F, P_H, P_R, P, Pr_f, Pr_g, Re_f, Re_{fo}, Re_g, Re_{go}, Su_f, Su_g, Su_{fo}, Su_{go}, We_f, We_{fo}, We_g, We_{go}, X_{tt}, X_{tv}, X_{vv}, β, D_h, h_{fg},k_f, k_g, G, x, T, μ_f, μ_g, σ	ANN	6.12	0.98	0.98
		Random Forest	16.54	0.90	0.90
		AdaBoost	33.49	0.77	0.76
		XGBoost	8.36	0.97	0.97
5	Bd, Co, Fr_f, Fr_{fo}, Fr_g, Fr_{go}, Ga, Ka, Pr_f, Pr_g, Re_f, Re_{fo}, Re_g, Re_{go}, Su_f, Su_g, Su_{fo}, Su_{go}, We_f, We_{fo}, We_g, We_{go}	ANN	6.80	0.98	0.98
		Random Forest	18.56	0.87	0.87
		AdaBoost	34.60	0.75	0.74
		XGBoost	9.06	0.97	0.97

(Case 2) give *MAEs* of 40.7% and 14.9%, respectively. As expected, this shows that the limited parameter selection is not sufficient enough to capture the condensation heat transfer coefficient information. Now, considering a set of input parameters that include all the flow parameters, the geometric parameters, and the fluid properties (Case 3) gives an MAE of 6.2%. Similarly, if we consider all the input parameters taken together including non-dimensional numbers (Case 4) we get an MAE of 6.1%. Both the cases show the model being able to capture the heat transfer behavior very accurately. Finally, with a model just based on all the dimensionless parameters relevant to condensation (Case 5), we get a slightly higher but still low MAE of 6.8%. The corresponding R^2 and adjusted R^2 are 0.98 and 0.98, respectively. While Cases 3 and 4 show a slightly lower MAE, we will utilize the all-dimensionless input parameter model as the final model for further analysis. There are two reasons for this. Firstly, to develop general two-phase flow predicting tools, the dimensionless parameters are the only set of parameters that provide a consistent comparison across working fluids, with geometric and fluid parameter variation. In addition, selecting a model with more input parameters like that done in Case 3 increases redundancies as the dimensionless parameters are calculated based on the other input parameters making those models less useful. Therefore, ANN model with input parameters: Bd, Co, Fr_f, Fr_{fo}, Fr_g, Fr_{go}, Ga, Ka, Pr_f, Pr_g, Re_f, Re_{fo}, Re_g, Re_{go}, Su_f, Su_g, Su_{fo}, Su_{go}, We_f, We_{fo}, We_g, and We_{go}, is selected. The corresponding Pearson's correlation coefficient map for the input parameters and the output parameter, h, is shown in Fig. 3. Fig. 4(a) shows the ANN model selected with input parameters: Bd, Co, Fr_f, Fr_{fo}, Fr_g, Fr_{go}, Ga, Ka, Pr_f, Pr_g, Re_f, Re_{fo}, Re_g, Re_{go}, Su_f, Su_g, Su_{fo}, Su_{go}, We_f, We_{fo}, We_g, and We_{go}, and hidden layers (150,140,130,120,110,100,90,80,70,60,50,40,30,20,10), and the corresponding comparison between the predicted and experimental heat transfer coefficient data is shown in Fig. 4(b). While the *MAE* is 6.8%, the percentage data predicted within ±30% is 97.8% and percentage data predicted within ±50% is 99.8%. The results show how well the model can capture the heat transfer behavior across the whole range of condensation heat transfer coefficient consolidated data. This result is not unexpected as ANNs have shown a lot of success with prior research in heat transfer analysis [38,40,41,44,46], including in a recent study on saturated flow boiling heat transfer coefficient prediction [45].

Table 5 also compares the predicting performance for the tree-based models based on different combinations of input parameters. When we look at the predictions of the other three machine-learning models, they follow the same trend in terms of predicting performance variation with input parameter selection as that of the ANN model. Therefore, the same set of dimensionless parameters as that selected for ANN are selected for further investigation for the tree based models.

Fig. 5(a) shows the comparison between the predicted and experimental heat transfer coefficient data based on the AdaBoost model. This model gives an *MAE* of 34.5% and percentage data predicted within ±30% is 63.6% and percentage data predicted within ±50% is 78.0%. This performance of the optimized AdaBoost model is inferior to the ANN model results shown in Fig. 4(b). This can be attributed to tree-based models doing better with categorical predictors [95], none of which were included in this model. All input parameters selected in this study were numeric, and for the current model, specifically, they are non-dimensional numbers. Fig. 5(b) shows the plots for feature importance, obtained for the AdaBoost model, showing ten parameters having the highest impact on the condensation heat transfer coefficient, h. The two parameters, vapor Froude number, Fr_g, and fluid only Froude number, Fr_{fo}, show the highest impact of 40% and 33%, respectively. This result is in line with the Pearson's correlation coefficient map in Fig. 3 that shows a high correlation of heat transfer coefficient with Froude numbers. Other important parameters in the order of impact include the Vapor Weber number, We_g, vapor Prandtl number, Pr_g, fluid only Reynolds number, Re_{fo}, and liquid Prandtl number, Pr_f, with impact between 4% and 6%.

Fig. 6(a) shows the comparison between the predicted and experimental heat transfer coefficient data based on the Random Forest model. This model gives *MAE* of 18.8% and percentage data predicted within ±30% is 84.4% and percentage data predicted within ±50% is 93.9%. The predictions of this optimized Random Forest model are better than what was obtained with AdaBoost but falls short of the ANN model. Fig. 6(b) shows the plots for feature importance, obtained for the Random Forest model, showing ten parameters having the highest impact on the condensation heat transfer coefficient, h. The two parameters, vapor Froude number, Fr_g, and fluid only Froude number, Fr_{fo}, show the highest impact of 58% and 19%, respectively. These two parameters of highest importance are same as those in the AdaBoost model. However, the feature importance is captured differently. Other important parameters in the order of impact include the vapor Prandtl number, Pr_g

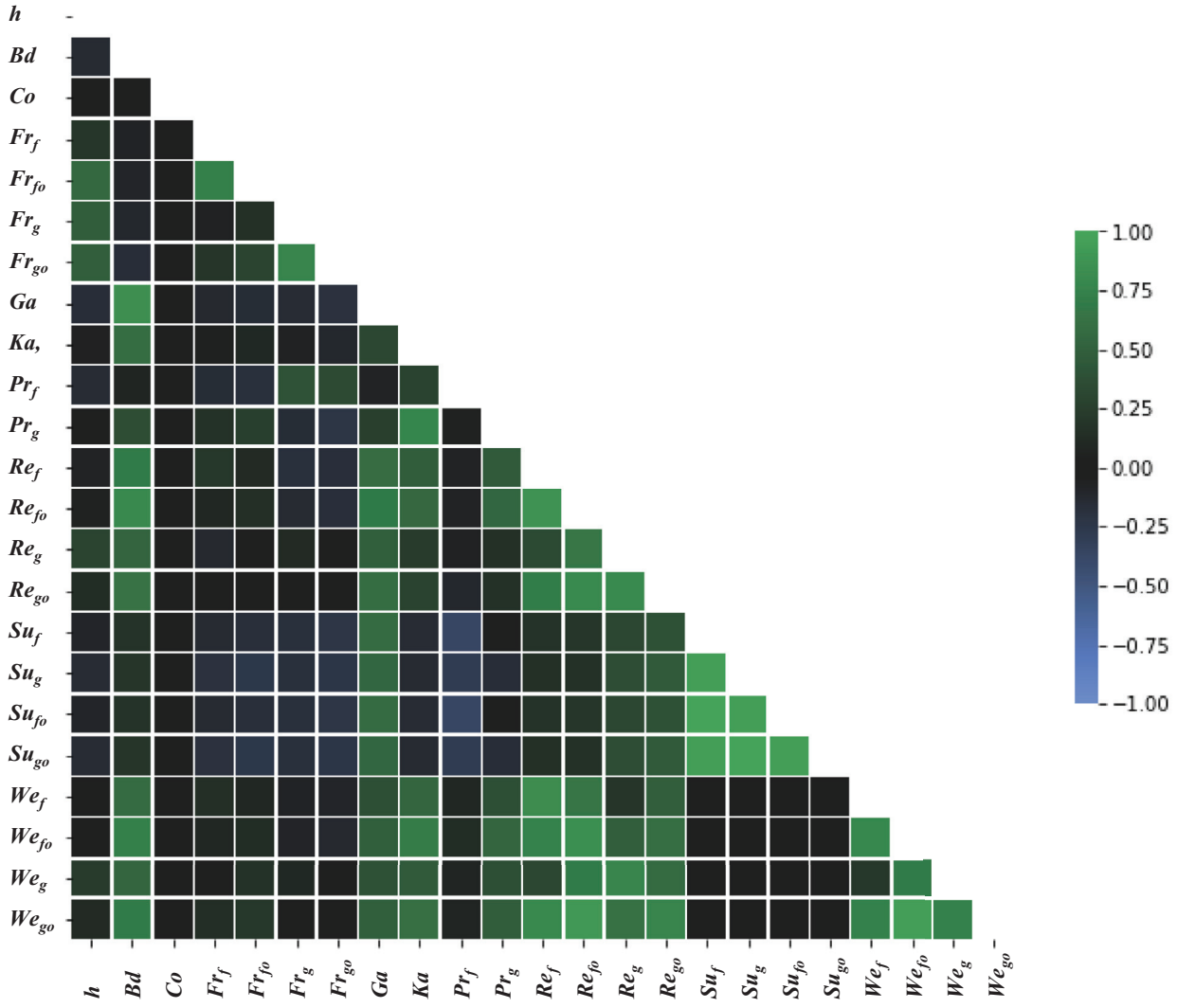

Fig. 3. Pearson's correlation coefficient map for input paramaters, *Bd*, *Co*, Fr_f, Fr_{fo}, Fr_g, Fr_{go}, *Ga*, *Ka*, Pr_f, Pr_g, Re_f, Re_{fo}, Re_g, Re_{go}, Su_f, Su_g, Su_{fo}, Su_{go}, We_f, We_{fo}, We_g, and We_{go} and output parameter, *h*.

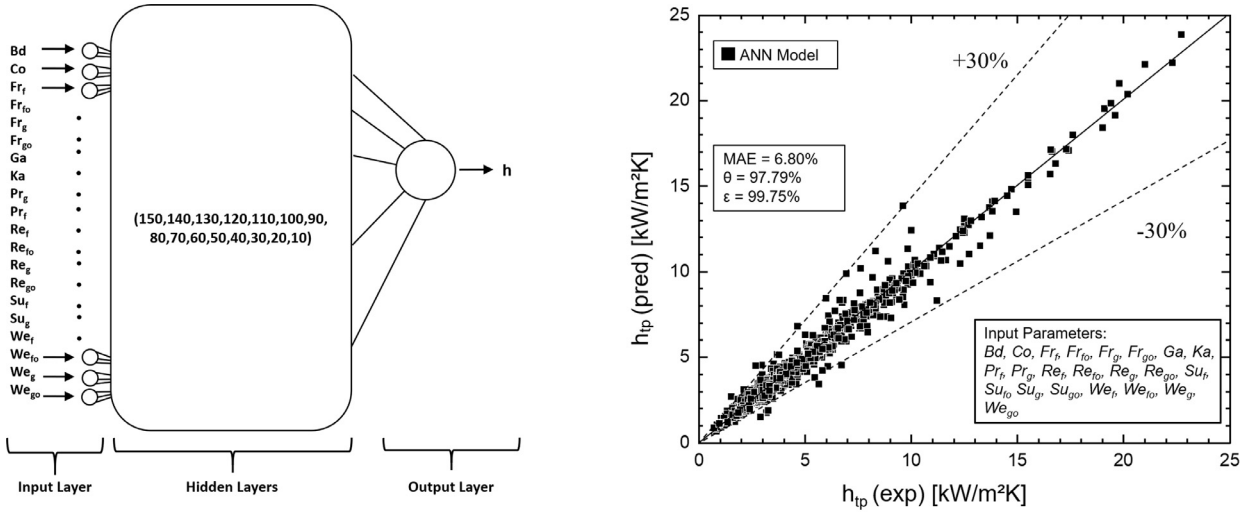

(a) (b)

Fig. 4. (a) ANN architecture with input, hidden and output layers selected as the final model for this study. (b) ANN model predictions based on the input parameters Bd, Co, Fr_f, Fr_{fo}, Fr_g, Fr_{go}, Ga, Ka, Pr_f, Pr_g, Re_f, Re_{fo}, Re_g, Re_{go}, Su_f, Su_{fo}, Su_g, Su_{go}, We_f, We_{fo}, We_g, and We_{go}.

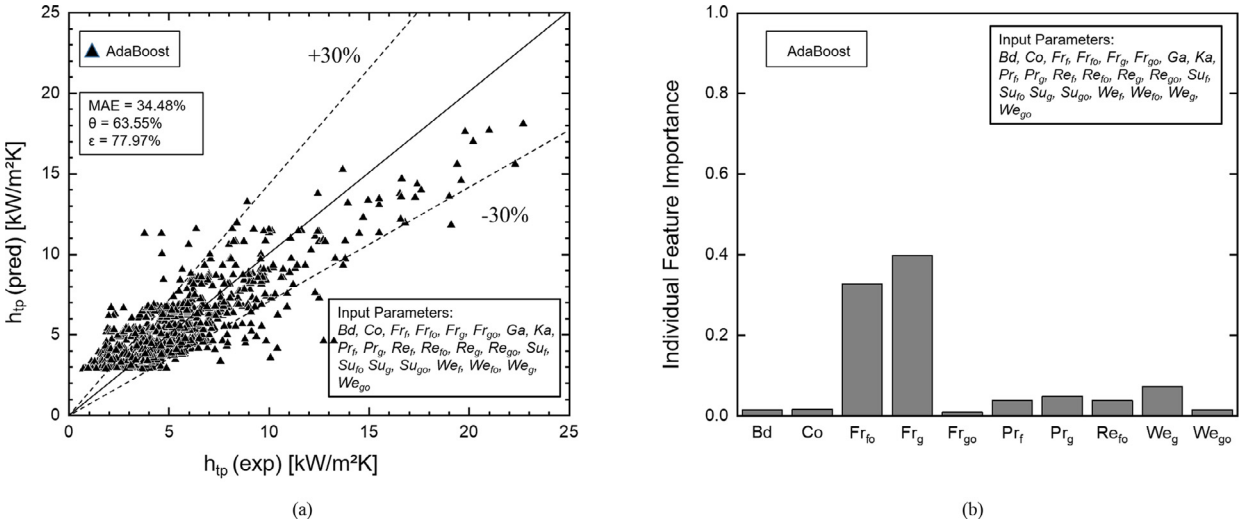

Fig. 5. (a) AdaBoost model predictions with input parameters Bd, Co, Fr_f, Fr_{fo}, Fr_g, Fr_{go}, Ga, Ka, Pr_f, Pr_g, Re_f, Re_{fo}, Re_g, Re_{go}, Su_f, Su_{fo}, Su_g, Su_{go}, We_f, We_{fo}, We_g, and We_{go}. (b) Feature importance plot based on the AdaBoost model.

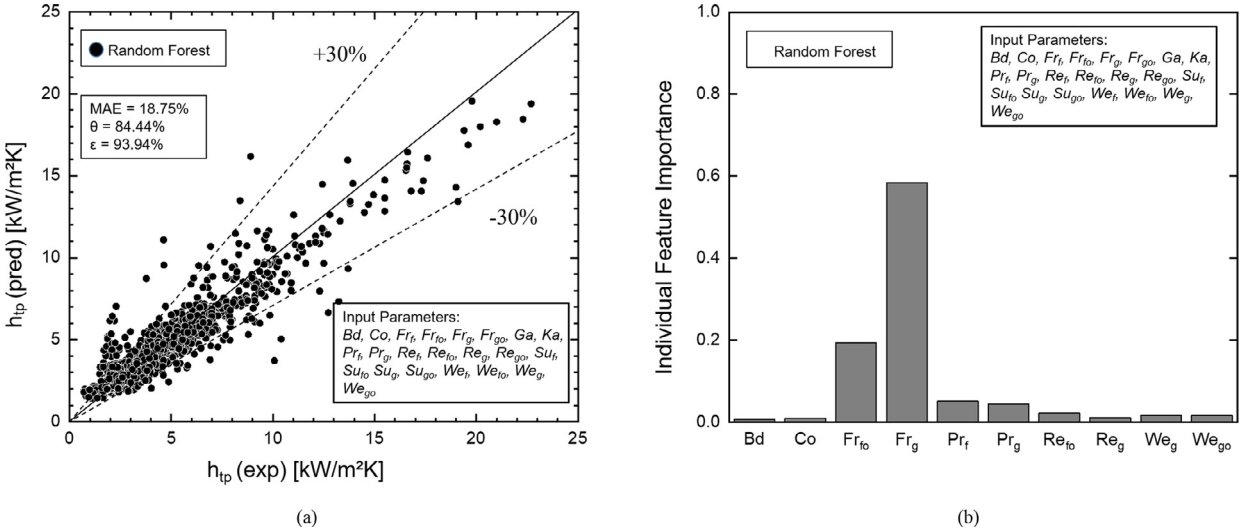

Fig. 6. (a) Random Forest model predictions with input parameters Bd, Co, Fr_f, Fr_{fo}, Fr_g, Fr_{go}, Ga, Ka, Pr_f, Pr_g, Re_f, Re_{fo}, Re_g, Re_{go}, Su_f, Su_{fo}, Su_g, Su_{go}, We_f, We_{fo}, We_g, and We_{go}. (b) Feature importance plot based on Random Forest model.

and liquid Prandtl number, Pr_f with both having impacts of around 4–5%.

Fig. 7(a) shows the comparison between the predicted and experimental heat transfer coefficient data based on the XGBoost model. This model gives *MAE* of 9.1% and percentage data predicted within ±30% is 96.0% and percentage data predicted within ±50% is 98.9%. The predictions of this model is comparable to the ANN model as shown in Fig. 4(b). Prior work in literature reports that both ANN and XGBoost models perform better than other machine learning models with XGBoost outperforming ANN when there are categorical predictors and response variables [100,101] in the data set. Fig. 7(b) shows the plots for feature importance, obtained for the XGBoost model, showing ten parameters having the highest impact on the condensation heat transfer coefficient, *h*. The two parameters, vapor Froude number, Fr_g, and fluid only Froude number, Fr_{fo}, show the highest impact of 37% and 17%, respectively. Other important parameters in the order of impact include the fluid only Reynolds number, Re_{fo}, vapor Prandtl number, Pr_g, vapor only Weber number, We_{go}, liquid Prandtl number, Pr_f with impact between 5% and 8%. While the same parameters show the highest importance as those seen with results from the AdaBoost and the Random Forest models, the XGBoost model's ability to capture the trends can be better trusted due to the lower *MAE* in heat transfer coefficient predictions.

In general, the results from the three tree-based models all show that Fr_g and Fr_{fo} have the highest impact on the heat transfer predictions. This result is significant because several prior correlations developed for condensation do not have these two parameters in their formulations [9–17]. The machine learning models do not explore or assume any underlying physics of the problem as predicated in correlations, but they learn the predicting behavior from the training data instead. Fig. 3 shows the Pearson's correlation coefficient between all the dimensionless predictors along with the heat transfer coefficient. Including highly correlated variables doesn't provide any benefit to model performance and are often handled naturally by getting dropped in several tree based algorithms [96]. Furthermore to support this, we see that the Pearson's correlation coefficient between the heat transfer coefficient and Fr_g, Fr_{fo} and Fr_{go} are 0.479, 0.561 and 0.484 respectively, showing strongest correlation with the target variable ('*h*') than any

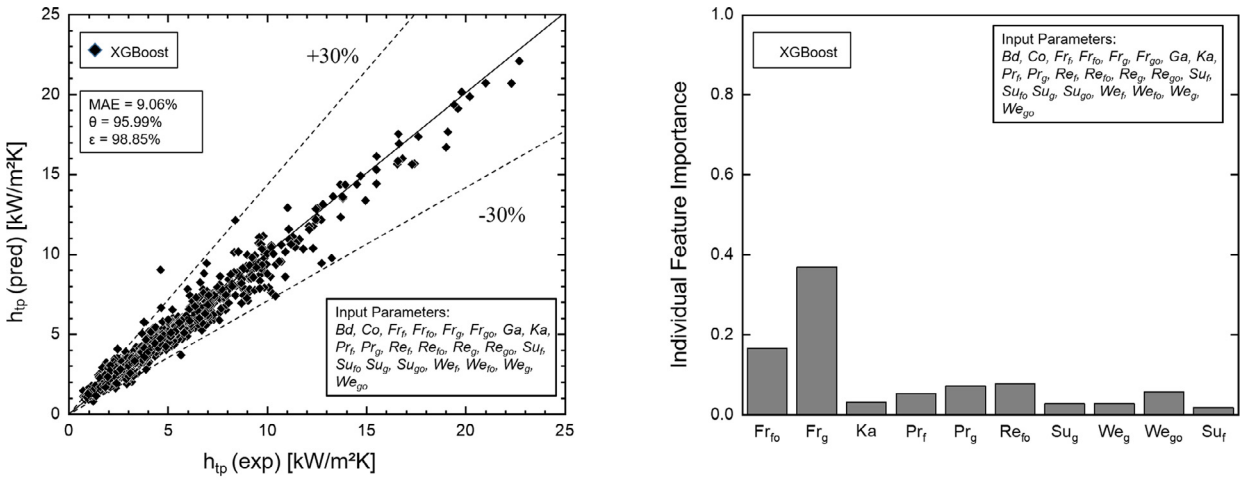

Fig. 7. (a) XGBoost model predictions with input parameters Bd, Co, Fr_f, Fr_{fo}, Fr_g, Fr_{go}, Ga, Ka, Pr_f, Pr_g, Re_f, Re_{fo}, Re_g, Re_{go}, Su_f, Su_{fo}, Su_g, Su_{go}, We_f, We_{fo}, We_g, and We_{go}. (b) Feature importance plot based on the XGBoost model.

other variable. This has led to these features being prime candidates to build the trees. However, correlation between Fr_g and Fr_{go} is high (0.767) and hence one of the two (Fr_{go} in this case) has been dropped from feature importance list. The feature importance result is not saying that physically, Froude numbers need to have a higher impact, and that the empirical correlation based predicting two-phase heat transfer tools are not accurate. Such high correlations between any two variables can occur and have been reported as 'Spurious Correlation' in the literature [102,103]. It does however tell us the bias of the available consolidated data, showing that it may have some higher significance to the heat transfer behavior than what is currently understood.

Going forward, we select the two best models, the ANN model and the XGBoost model for further discussion because these two models performed significantly better than the other two models that are investigated, the Random Forest model and the AdaBoost model.

3.2. Comparison with generalized condensation heat transfer correlations

The ANN and XGBoost model results based on the test dataset were compared with predictions of the generalized corrections by Shah [25] and Kim and Mudawar [26]. Table 6 provides the formulations of these generalized flow condensation heat transfer correlations. As illustrated in Fig. 8(a), the *MAE* for Shah [25] is 40.0% and percentage data predicted within ±30% is 48.0% and percentage data predicted within ±50% is 71.7%. Because this generalized correlation was developed for primarily larger sized flow channels with only 23% of the data falling in the hydraulic diameter range under investigation in this study, the inferior performance is expected and is not an assessment of the correlation itself. As shown in Fig. 8(b), the *MAE* for Kim and Mudawar [26] is 26.6% and percentage data predicted within ±30% is 65.4% and percentage data predicted within ±50% is 91.4%. The correlation by Kim and Mudawar [26] was also developed for a limited range of parameters than those used in this study, which is the reason for the slightly higher *MAE* that that reported in their study. Overall, the ANN and XGBoost models' predicting capability is superior to both the generalized correlations.

Another measure to understand the model performance is its ability to capture individual datasets with comparable accuracy. Fig. 9(a–d) shows the ANN model predictions vs. experimental data for the four largest databases used in the consolidated data. Wang [79], which was the largest database with R134a as the working fluid, has *MAE* of 7.0%, and the percentage data predicted within ±30% is 99.5% and percentage data predicted within ±50% is 100%. Similarly, Kim and Mudawar [77] based on FC-72 as the working fluid has *MAE* of 5.3%, and the percentage data predicted within ±30% is 98.4% and percentage data predicted within ±50% is 100.0%. In general, the ANN model did well for all four databases. These databases include a good variation of geometric and operating parameters with 7 working fluids: R134a, R245fa, R410a, and FC-72, mass velocity: 67 – 800 kg/m²s, hydraulic diameter: 0.76 – 3.05 mm, reduced pressure: 0.057 – 0.92, quality: 0 – 1.0, and fluid only Reynolds number: 303 – 44033. Fig. 9(e–h) shows the XGBoost model predictions vs. experimental data for the four largest databases used in the consolidated data. Results show similar trends as that observed with ANN model results. These plots clearly show that both the ANN model and XGBoost model predictions are superior to the consolidated correlation by Kim and Mudawar [26].

Flow condensation in mini/micro-channel sees multiple flow regimes but most of the data can be majorly subdivided into either (1) slug and bubble flow- or (2) annular flow regimes as stated in [26]. While the machine learning models are oblivious to the transition point, the correlation by Kim and Mudawar [26] defines a specific criterion as shown in Table 6. Using this criterion, when we compare the performance with respect to the specific flow regimes as shown in Fig. 10(a–d), the ANN and XGBoost models show that their performances are better than the consolidated correlation by Kim and Mudawar [26] in both the flow regimes.

3.3. Predicting excluded databases

All the previous results discussed in this study were based on the machine-learning algorithms trained by using randomly selected training data from 37 data sources [47–83]. However, a robust predicting tool for two-phase flows is only useful to design engineers if it has the ability to predict data points outside its training space. Here, we compare model performance for the optimized ANN and XGBoost models by excluding databases and predicting the corresponding condensation heat transfer coefficients. Three databases were excluded one by one, such that we have one case with a fluid that is commonly repeating in the training databases, one case with a fluid repeating just once in the training

Table 6
Generalized condensation heat transfer correlations.

Author(s)	Correlation Formulations
Shah [25]	For vertical and inclined tubes Regime I $J_g \geq \frac{1}{2.4Z+0.73}$ Regime II $J_g \geq 0.89 - 0.93\exp(-0.087Z^{-1.17})$ Regime III $J_g \leq 0.89 - 0.93\exp(-0.087Z^{-1.17})$\ Where $J_g = \frac{xG}{(gD\rho_g(\rho_l-\rho_g))^{0.5}}$ For horizontal tubes Regime I $J_g \geq 0.98(Z+0.263)^{-0.62}$ Regime II $J_g \leq 0.98(Z+0.263)^{-0.62}$ For all tube orientations (except upward flow) In Regime I $h_{TP} = h_l$ In Regime II $h_{TP} = h_l + h_{Nu}$ For horizontal tubes, Regime II occurs when $Re_{GT} \geq 35000$. For vertical tubes in Regime III $h_{TP} = h_{Nu}$ Where $h_l = h_{LT}(\frac{\mu_f}{14\mu_g})^n[(1-x)^{0.8} + \frac{3.8x^{0.76}(1-x)^{0.04}}{Pr^{0.38}}]$ $n = 0.0058 + 0.557\,Pr$ $h_{Nu} = 1.32Re_{LS}^{-1/3}[\frac{\rho_l(\rho_l-\rho_g)gk_f^3}{\mu_f^2}]^{1/3}$
Kim and Mudawar [26]	For annular flow (smooth-annular, wavy-annular, transition) where $We^* > 7X_{tt}^{0.2}$: $\frac{h_{ann}D_h}{k_f} = 0.048Re_f^{0.69}Pr_f^{0.34}\frac{\phi_g}{X_{tt}}$. For slug and bubbly flows where $We^* < 7\,X_{tt}^{0.2}$: $\frac{h_{non-ann}D_h}{k_f} = [(0.048\mathrm{Re}_f^{0.69}\,\mathrm{Pr}_f^{0.34}\,\frac{\phi_g}{X_{tt}})^2 + (3.2\times10^{-7}\mathrm{Re}_f^{-0.38}Su_{go}^{1.39})^2]^6$. where$X_{tt} = (\frac{\mu_f}{\mu_g})^{0.1}(\frac{1-x}{x})^{0.9}(\frac{\rho_g}{\rho_f})^{0.5}$, $\phi_g^2 = 1 + CX + X^2$, $X^2 = \frac{(dP/dz)_f}{(dP/dz)_g}$, $-(\frac{dP}{dz})_f = \frac{2f_f v_f G^2(1-x)^2}{D_h}$, $-(\frac{dP}{dz})_g = \frac{2f_g v_g G^2 x^2}{D_h}$, $f_k = 16Re_k^{-1}$for$Re_k < 2,000$, $f_k = 0.079Re_k^{-0.25}$for$2,000 \leq Re_k < 20,000$, $f_k = 0.046Re_k^{-0.2}$for$Re_k \geq 20,000$, For laminar flow in rectangular channel (β <1), $f_kRe_k = 24(1 - 1.3553\,\beta + 1.9467\,\beta^2 - 1.7012\,\beta^3 + 0.9564\,\beta^4 - 0.2537\,\beta^5)$, where subscript k denotes f or g for liquid and vapor phases, respectively, $\mathrm{Re}_f = \frac{G(1-x)D_h}{\mu_f}$, $Re_g = \frac{GxD_h}{\mu_g}$, $Re_{fo} = \frac{GD_h}{\mu_f}$,$Su_{go} = \frac{\rho_g\sigma D_h}{\mu_g^2}$.

Liquid	Vapor (gas)	C
Turbulent	Turbulent	$0.39Re_{fo}^{0.03}Su_{go}^{0.10}(\frac{\rho_f}{\rho_g})^{0.35}$for $Re_f \geq 2000$, $\mathrm{Re}_g \geq 2000$ (tt)
Turbulent	Laminar	$8.7\times10^{-4}Re_{fo}^{0.17}Su_{go}^{0.50}(\frac{\rho_f}{\rho_g})^{0.14}$for $Re_f \geq 2000$, $\mathrm{Re}_g < 2000$ (tv)
Laminar	Turbulent	$0.0015Re_{fo}^{0.59}Su_{go}^{0.19}(\frac{\rho_f}{\rho_g})^{0.36}$for $Re_f < 2000$, $\mathrm{Re}_g \geq 2000$ (vt)
Laminar	Laminar	$3.5\times10^{-5}Re_{fo}^{0.44}Su_{go}^{0.50}(\frac{\rho_f}{\rho_g})^{0.48}$for $Re_f < 2000$, $\mathrm{Re}_g < 2000$ (vv)

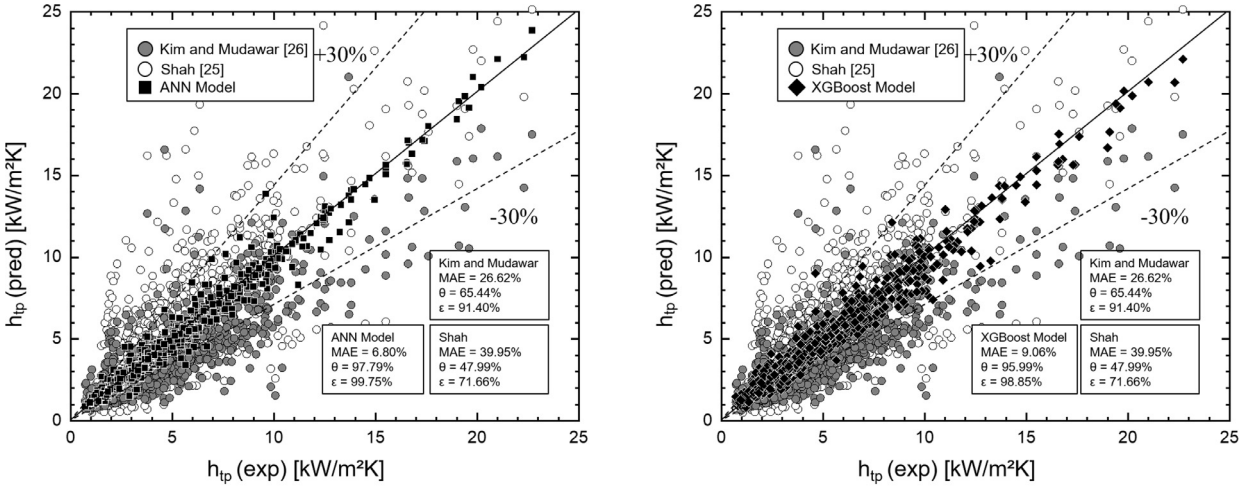

Fig. 8. Comparison between predictions of the generalized corrections by Shah [25] and Kim & Mudawar [26] with test data predictions based on the (a) ANN model and (b) XGBoost model.

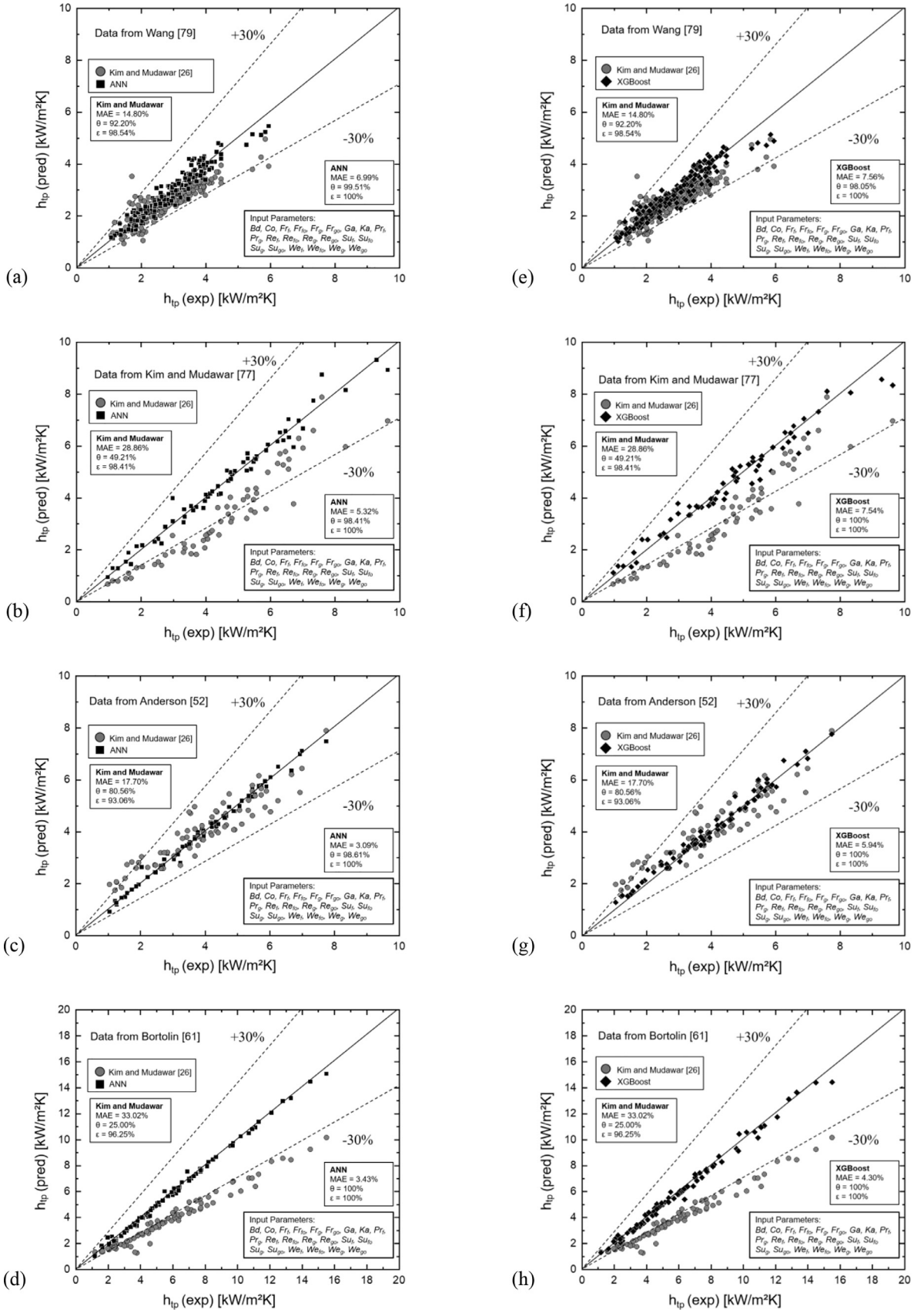

Fig. 9. ANN model predicting test data points from individual databases of (a) Wang [79], (b) Kim and Mudawar [77], (c) Andresen [52], and (d) Bortolin [61]. XGBoost model predicting test data points from individual databases of (e) Wang [79], (f) Kim and Mudawar [77], (g) Andresen [52], and (h) Bortolin [61].

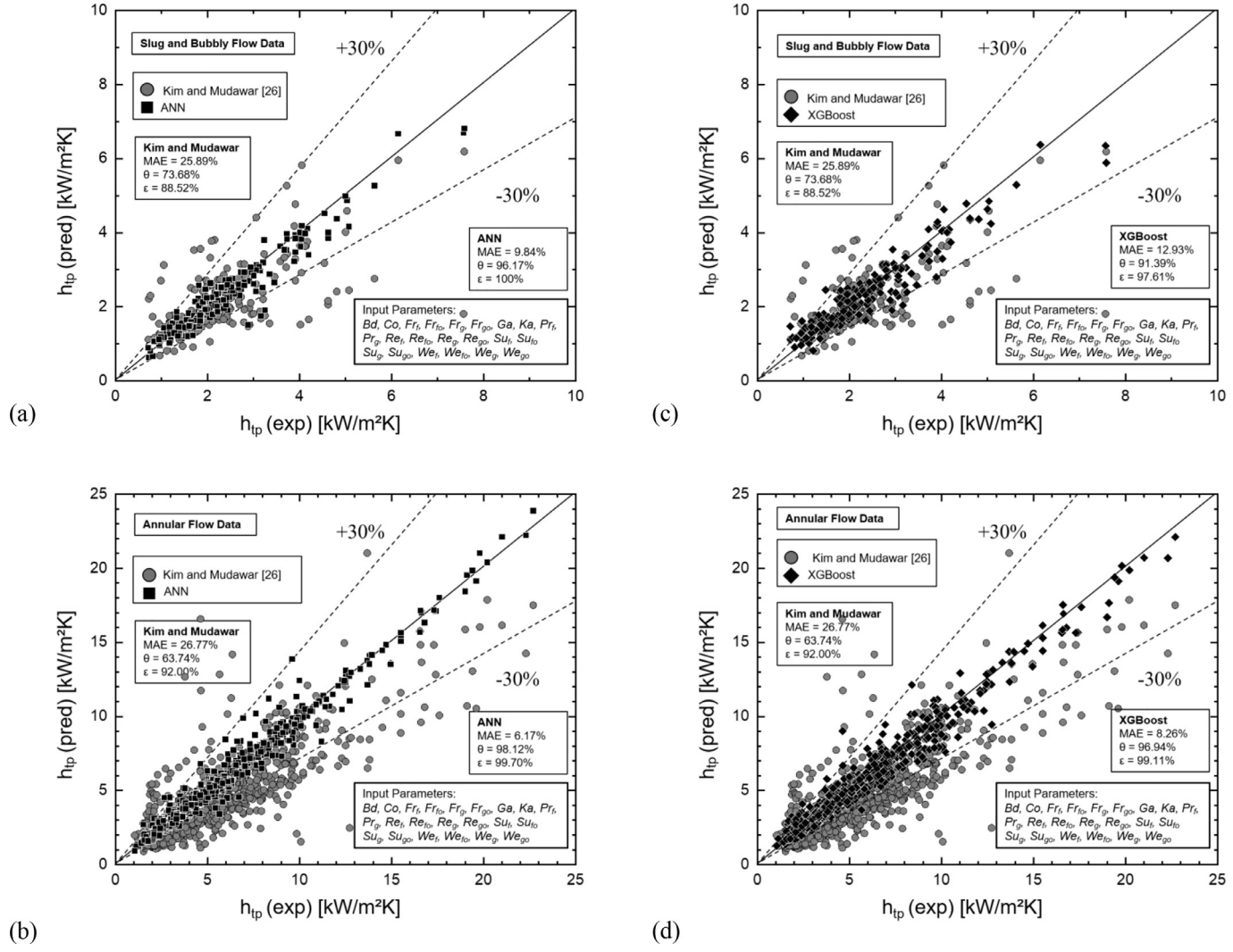

Fig. 10. (a) ANN model predictions for slug and bubbly flow test data. (b) ANN model predictions for annular flow test data. (c) XGBoost model predictions for slug and bubbly flow test data. (d) XGBoost model predictions for annular flow test data.

databases, and one case with no fluid information in the training databases.

Fig. 11 (a–b) shows the ANN model and XGBoost model predictions when Wang [79], the largest database from the consolidated data, is excluded from the training database that consisted of the 36 remaining sources [47–78,80–83]. For ANN model and XGBoost model, the results show that even though this was a large database that was excluded, *MAEs* were as low as 13.5%, and 16.8%, respectively. We can see that in Table 1, R134a is investigated by many researchers over a large range of geometric and operating parameters, thus the reason for a low *MAE*. Fig. 12(a) and (b) shows the experimental data and corresponding predictions of local heat transfer coefficient vs. vapor quality for some selected data from Wang [79] for ANN model and XGBoost model, respectively. For a range of mass velocities, saturation temperatures and vapor qualities, the models can predict not only the local values but also capture the trends in condensation heat transfer coefficients with vapor quality.

Fig. 11 (c–d) shows the ANN model and XGBoost model predictions when Gomez et al. [73] is excluded from the training database that consisted of the 36 remaining sources [47–72,74–83]. For ANN model and XGBoost model, the results show that *MAEs* were 17.8%, and 14.8%, respectively. The data for the fluid, R1234yf, is only available in one other training database, however, this fluid has many similar properties to R134a [104], thus the models is able to capture the behavior to a certain degree. Fig. 12(c) and (d) shows the experimental data and corresponding predictions of local heat transfer coefficient vs. vapor quality for some selected data from Gomez et al. [73] for ANN model and XGBoost model, respectively. Here, the models show them capturing the trends but not the local values as well as the last case with Wang [79].

Fig. 11 (e–f) shows the ANN model and XGBoost model predictions when Kim and Mudawar [77] is excluded from the training database that consisted of the 36 remaining sources [47–76,78–83]. The working fluid in Kim and Mudawar [77] was FC-72. The results show that both the ANN model and XGBoost model did an extremely poor job with *MAE* of 77.1% and 37.6%, respectively. This can be attributed to the fluid information not being available for training, and the models not capturing the heat transfer variation accurately in cases where working fluid information is not in the training database.

The results show a strong dependence of model performance on availability of fluid data in the training datasets. This is a shortcoming expected of machine learning methods having high reliability on availability of prior data. In spite of that, the machine learning models show a reasonably good predicting capability. The current shortcoming can be addressed over time by amassing more data for more working fluids that include more geometric and

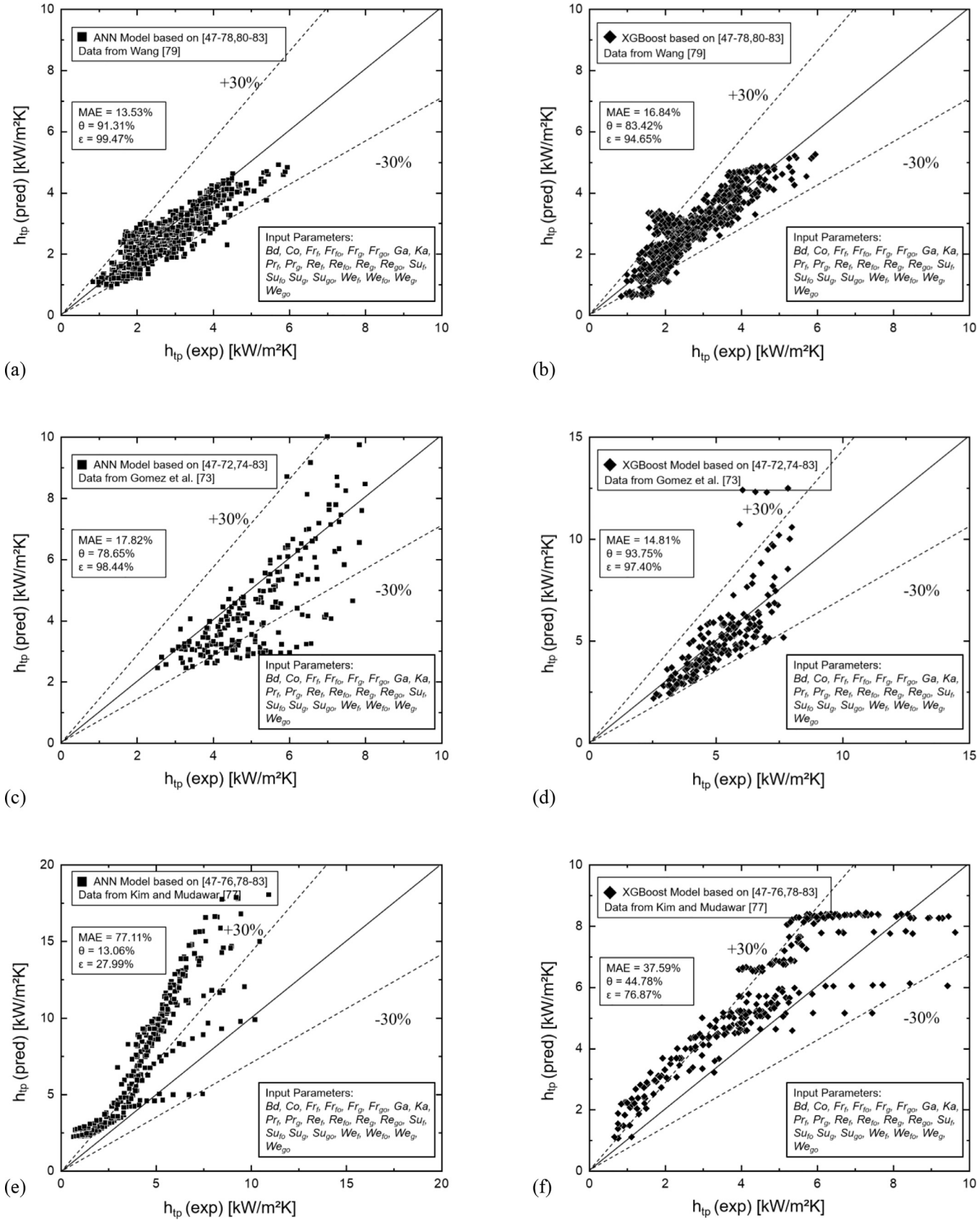

Fig. 11. Predictions of heat transfer coefficients of excluded data for (a) Wang [79] based on the ANN model, (b) Wang [79] based on the XGBoost model, (c) Gomez et al. [73] based on the ANN model. (d) Gomez et al. [73] based on the XGBoost model, (e) and Kim and Mudawar [77] based on the ANN model, and (f) Kim and Mudawar [77] based on the XGBoost model.

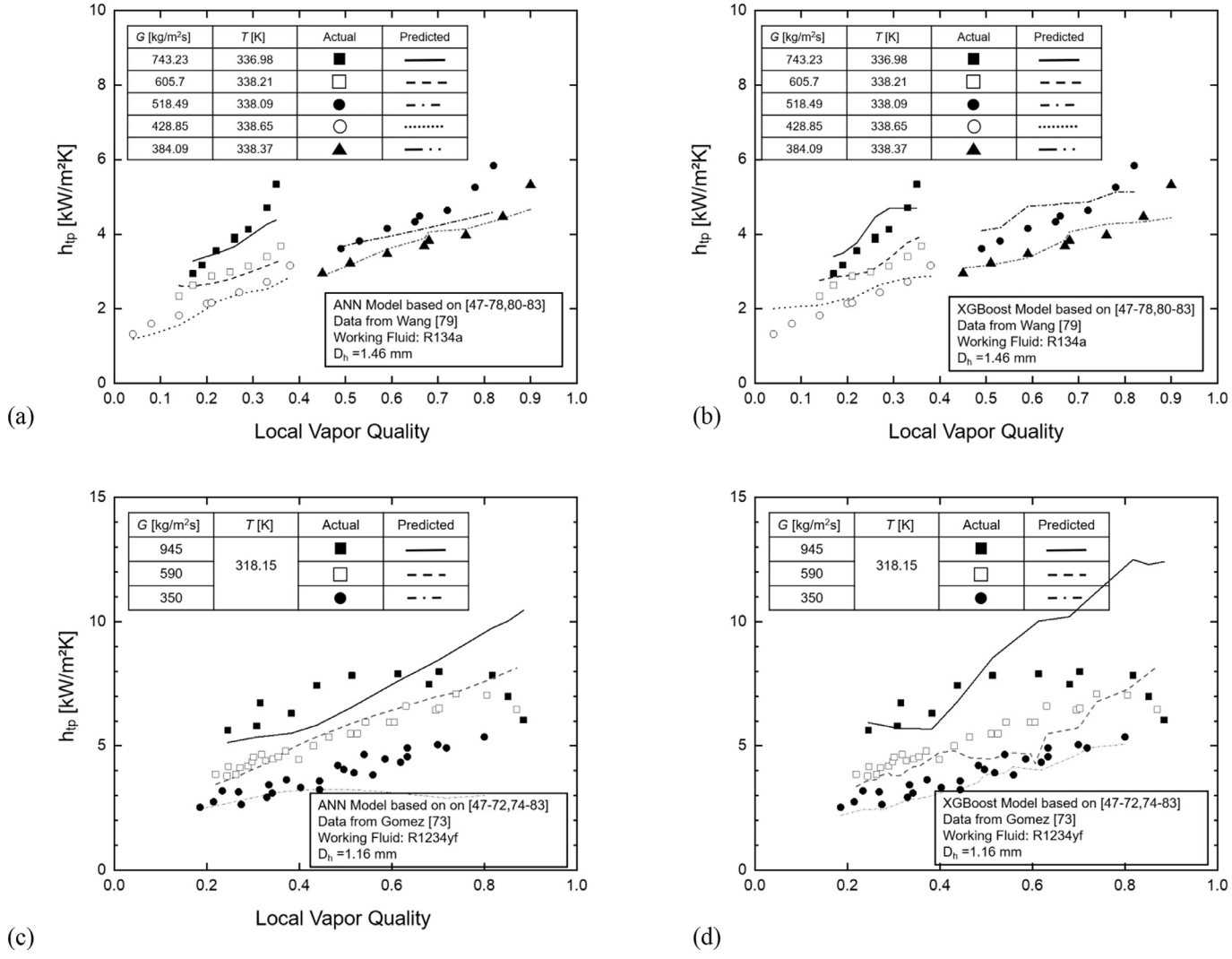

Fig. 12. Local heat transfer coefficients vs. vapor quality of excluded data for (a) Wang [79] based on the ANN model, (b) and Wang [79] based on the XGBoost model, (c) Gomez et al. [73] based on the ANN model, (d) and Gomez et al. [73] based on the XGBoost model.

parametric variations than that included in the current consolidated database.

4. Conclusions

In this study, a new method for predicting heat transfer coefficient for flow condensation in mini/micro channels is proposed. A consolidated database of flow condensation heat transfer is amassed and utilized to develop machine learning based approaches for predicting the data. Key findings from this study are as follows:

(1) A consolidated database of 4,882 data points for flow condensation heat transfer in mini/micro-channels is amassed from 37 sources that includes 17 working fluid, reduced pressures of 0.039 – 0.916, hydraulic diameters of 0.424 mm – 6.52 mm, mass velocities of $50 < G < 1403$ kg/m^{2}s, liquid-only Reynolds numbers of 285 – 89,797, superficial vapor Reynolds number of 44 – 389,298, and flow qualities of 0 – 1.

(2) Four machine learning based models, namely, Artificial Neural Networks, Random Forest, Adaptive Boost and Extreme Gradient Boosting were developed and compared for predicting accuracy. A parametric optimization is conducted which showed that the ANN and XGBoost models showed the best predicting accuracy. Based on dimensionless input parameters, *Bd, Co, Fr$_f$, Fr$_{fo}$, Fr$_g$, Fr$_{go}$, Ga, Ka, Pr$_f$, Pr$_g$, Re$_f$, Re$_{fo}$, Re$_g$, Re$_{go}$, Su$_f$, Su$_g$, Su$_{fo}$, Su$_{go}$, We$_f$, We$_{fo}$, We$_g$,* and *We$_{go}$* the ANN model and the XGBoost model predicted the test data with *MAEs* of 6.8% and 9.1%, respectively.

(3) The optimal ANN and XGBoost models performed better than the highly reliable universal generalized flow condensation correlation in mini/micro-channels by Kim and Mudawar [26]. The models not only captured heat transfer coefficients well for individual datasheets, but also for different condensation flow regimes.

(4) To check the predicting performance of the ANN and XGBoost models for datasets outside its training database, certain datasets were completely excluded, and the models were used to predict the excluded data. Reasonable accuracy in predicting the heat transfer coefficients and the trends of heat transfer coefficient with vapor quality was seen when data points including the specific working fluid were part of the training dataset of the remaining datasheets. The accuracy of the models was compromised when no fluid specific information was available in the training dataset.

(5) The results of this study show that machine learning algorithms can help develop a robust new predicting tool for condensation heat transfer coefficients in mini/micro channels.

Declaration of Competing Interest

We wish to confirm that there are no known conflicts of interest associated with this publication and there has been no significant financial support for this work that could have influenced its outcome.

CRediT authorship contribution statement

Liwei Zhou: Formal analysis, Investigation, Data curation. **Deepak Garg:** Conceptualization, Methodology, Software, Writing - original draft. **Yue Qiu:** Validation, Investigation. **Sung-Min Kim:** Data curation, Methodology, Writing - review & editing. **Issam Mudawar:** Methodology, Writing - review & editing. **Chirag R. Kharangate:** Conceptualization, Methodology, Supervision, Writing - original draft, Writing - review & editing.

References

[1] T.N. Tran, M.W. Wambsganss, D.M. France, Small circular-and rectangular-channel boiling with two refrigerants, Int. J. Multiph. Flow. 22 (1996) 485–498.
[2] H.J. Lee, S.Y. Lee, Heat transfer correlation for boiling flows in small rectangular horizontal channels with low aspect ratios, Int. J. Multiph. Flow. 27 (2001) 2043–2062.
[3] D.C. Wadsworth, I. Mudawar, Enhancement of single-phase heat transfer and critical heat flux from an ultra-high-flux simulated microelectronic heat source to a rectangular impinging jet of dielectric liquid, J. Heat Transf. (Transactions ASME (American Soc. Mech. Eng. Ser. C) (1992) 114.
[4] Y. Katto, M. Kunihiro, Study of the mechanism of burn-out in boiling system of high burn-out heat flux, Bull. JSME. 16 (1973) 1357–1366.
[5] L. Lin, R. Ponnappan, Heat transfer characteristics of spray cooling in a closed loop, Int. J. Heat Mass Transf. 46 (2003) 3737–3746.
[6] J.G. Collier, J.R. Thome, Convective Boiling and Condensation, Clarendon Press, 1994.
[7] J.W. Coleman, S. Garimella, Two-phase flow regimes in round, square and rectangular tubes during condensation of refrigerant R134a, Int. J. Refrig. 26 (2003) 117–128.
[8] S.-M. Kim, J. Kim, I. Mudawar, Flow condensation in parallel micro-channels–part 1: experimental results and assessment of pressure drop correlations, Int. J. Heat Mass Transf. 55 (2012) 971–983.
[9] W.W. Akers, Condensation inside horizontal tubes, Chem. Engg. Prog. Symp. Ser. 56 (1960) 145.
[10] A. Cavallini, R. Zecchin, A dimensionless correlation for heat transfer in forced convection condensation, Proc. Sixth Int. Heat Transf. Conf. 3 (1974) 309–313.
[11] M.M. Shah, A general correlation for heat transfer during film condensation inside pipes, Int. J. Heat Mass Transf. 22 (1979) 547–556, doi:10.1016/0017-9310(79)90058-9.
[12] H. Haraguchi, Condensation of refrigerants HCFC22, HFC134a and HCFC123 in a horizontal smooth tube, Trans. Jpn. Soc. Mech. Eng. 60 (1994) 245–252.
[13] M.K. Dobson, J.C. Chato, Condensation in smooth horizontal tubes, J. Heat Transf. 120 (1998) 193–213, doi:10.1115/1.2830043.
[14] K.W. Moser, R.L. Webb, B. Na, A new equivalent Reynolds number model for condensation in smooth tubes, J. Heat Transf. 120 (1998) 410–417.
[15] W.-W.W. Wang, T.D. Radcliff, R.N. Christensen, A condensation heat transfer correlation for millimeter-scale tubing with flow regime transition, Exp. Therm. Fluid Sci. 26 (2002) 473–485.
[16] S. Koyama, K. Kuwahara, K. Nakashita, K. Yamamoto, An experimental study on condensation of refrigerant R134a in a multi-port extruded tube, Int. J. Refrig. 26 (2003) 425–432.
[17] T. Bohdal, H. Charun, M. Sikora, Comparative investigations of the condensation of R134a and R404A refrigerants in pipe minichannels, Int. J. Heat Mass Transf. 54 (2011) 1963–1974.
[18] S.-M. Kim, I. Mudawar, Theoretical model for annular flow condensation in rectangular micro-channels, Int. J. Heat Mass Transf. 55 (2012) 958–970.
[19] E. Da Riva, D. Del Col, Effect of gravity during condensation of R134a in a circular minichannel, Microgravity Sci. Technol. 23 (2011) 87.
[20] H. Ganapathy, A. Shooshtari, K. Choo, S. Dessiatoun, M. Alshehhi, M. Ohadi, Volume of fluid-based numerical modeling of condensation heat transfer and fluid flow characteristics in microchannels, Int. J. Heat Mass Transf. 65 (2013) 62–72.
[21] S. Chen, Z. Yang, Y. Duan, Y. Chen, D. Wu, Simulation of condensation flow in a rectangular microchannel, Chem. Eng. Process. Process Intensif. 76 (2014) 60–69.
[22] J. Zhang, W. Li, W.J. Minkowycz, Numerical simulation of condensation for R410A at varying saturation temperatures in mini/micro tubes, Numer. Heat Transf. Part A Appl. 69 (2016) 464–478.
[23] C.R. Kharangate, I. Mudawar, Review of computational studies on boiling and condensation, Int. J. Heat Mass Transf. (2017) 108, doi:10.1016/j.ijheatmasstransfer.2016.12.065.
[24] D. Lakehal, M. Fulgosi, G. Yadigaroglu, Direct numerical simulation of condensing stratified flow, J. Heat Transfer 130 (2008) 21501.
[25] M.M. Shah, An improved and extended general correlation for heat transfer during condensation in plain tubes, Hvac&R Res. 15 (2009) 889–913.
[26] S.-M. Kim, I. Mudawar, Universal approach to predicting heat transfer coefficient for condensing mini/micro-channel flow, Int. J. Heat Mass Transf. 56 (2013) 238–250.
[27] J. Friedman, T. Hastie, R. Tibshirani, The Elements of Statistical Learning, Springer series in statistics, New York, 2001.
[28] D.D. Massie, Optimization of a building's cooling plant for operating cost and energy use, Int. J. Therm. Sci. 41 (2002) 1121–1129, doi:10.1016/S1290-0729(02)01398-4.
[29] J. Yang, H. Rivard, R. Zmeureanu, On-line building energy prediction using adaptive artificial neural networks, Energy Build. 37 (2005) 1250–1259, doi:10.1016/J.ENBUILD.2005.02.005.
[30] A. Abbassi, L. Bahar, Application of neural network for the modeling and control of evaporative condenser cooling load, Appl. Therm. Eng. 25 (2005) 3176–3186, doi:10.1016/J.APPLTHERMALENG.2005.04.006.
[31] S. Lecoeuche, S. Lalot, B. Desmet, Modelling a non-stationary single tube heat exchanger using multiple coupled local neural networks, Int. Commun. Heat Mass Transf. 32 (2005) 913–922, doi:10.1016/J.ICHEATMASSTRANSFER.2004.08.029.
[32] G. Diáz, M. Sen, K.. Yang, R.L. McClain, Dynamic prediction and control of heat exchangers using artificial neural networks, Int. J. Heat Mass Transf. 44 (2001) 1671–1679, doi:10.1016/S0017-9310(00)00228-3.
[33] N. Bar, T.K. Bandyopadhyay, M.N. Biswas, S.K. Das, Prediction of pressure drop using artificial neural network for non-Newtonian liquid flow through piping components, J. Pet. Sci. Eng. 71 (2010) 187–194, doi:10.1016/J.PETROL.2010.02.001.
[34] G. Díaz, M. Sen, K.T. Yang, R.L. McClain, Simulation of heat exchanger performance by artificial neural networks, HVAC&R Res. 5 (1999) 195–208, doi:10.1080/10789669.1999.10391233.
[35] A. Pacheco-Vega, M. Sen, R.L. McClain, Analysis of fin-tube evaporator performance with limited experimental data using artificial neural networks, ASME-Publications-HTD 366 (2000) 95–102.
[36] M.W. Ahmad, M. Mourshed, Y. Rezgui, Trees vs neurons: comparison between random forest and ANN for high-resolution prediction of building energy consumption, Energy Build. 147 (2017) 77–89.
[37] J. Thibault, B.P.A. Grandjean, A neural network methodology for heat transfer data analysis, Int. J. Heat Mass Transf. 34 (1991) 2063–2070, doi:10.1016/0017-9310(91)90217-3.
[38] K. Jambunathan, S.L. Hartle, S. Ashforth-Frost, V.N. Fontama, Evaluating convective heat transfer coefficients using neural networks, Int. J. Heat Mass Transf. 39 (1996) 2329–2332, doi:10.1016/0017-9310(95)00332-0.
[39] P. Naphon, T. Arisariyawong, Heat transfer analysis using artificial neural networks of the spirally fluted tubes, J. Res. Appl. Mech. Eng. 4 (2016) 135–147.
[40] P. Naphon, T. Arisariyawong, T. Nualboonrueng, Artificial neural network analysis on the heat transfer and friction factor of the double tube with spring insert, Int. J. Appl. Eng. Res. 11 (2016) 3542–3549.
[41] A.M. Ghahdarijani, F. Hormozi, A.H. Asl, Convective heat transfer and pressure drop study on nanofluids in double-walled reactor by developing an optimal multilayer perceptron artificial neural network, Int. Commun. Heat Mass Transf. 84 (2017) 11–19, doi:10.1016/J.ICHEATMASSTRANSFER.2017.03.014.
[42] M. Mehrabi, M. Sharifpur, J.P. Meyer, Modelling and multi-objective optimisation of the convective heat transfer characteristics and pressure drop of low concentration TiO2-water nanofluids in the turbulent flow regime, Int. J. Heat Mass Transf. 67 (2013) 646–653, doi:10.1016/j.ijheatmasstransfer.2013.08.013.
[43] P. Naphon, S. Wiriyasart, T. Arisariyawong, Artificial neural network analysis the pulsating Nusselt number and friction factor of TiO2/water nanofluids in the spirally coiled tube with magnetic field, Int. J. Heat Mass Transf. 118 (2018) 1152–1159, doi:10.1016/j.ijheatmasstransfer.2017.11.091.
[44] P. Naphon, S. Wiriyasart, T. Arisariyawong, L. Nakharintr, ANN, numerical and experimental analysis on the jet impingement nanofluids flow and heat transfer characteristics in the micro-channel heat sink, Int. J. Heat Mass Transf. 131 (2019) 329–340, doi:10.1016/j.ijheatmasstransfer.2018.11.073.
[45] Y. Qiu, D. Garg, L. Zhou, C. Kharangate, S.-M. Kim, I. Mudawar, An artificial neural network model to predict mini/micro-channels saturated flow boiling heat transfer coefficient based on universal consolidated data, Int. J. Heat Mass Transf. (n.d.).
[46] A. Baghban, M. Kahani, M.A. Nazari, M.H. Ahmadi, W.-M. Yan, Sensitivity analysis and application of machine learning methods to predict the heat transfer performance of CNT/water nanofluid flows through coils, Int. J. Heat Mass Transf. 128 (2019) 825–835.
[47] M.K. Dobson, J.C. Chato, D.K. Hinde, S.P. Wang, Experimental evaluation of internal condensation of refrigerants R-134a and R-12, Air Conditioning and Refrigeration Center. College of Engineering …, 1993.
[48] M.K. Dobson, J.C. Chato, S.P. Wang, D.K. Hinde, J.A. Gaibel, Initial Condensation Comparison of R-22 With R-134a and R-321R-125, Air Conditioning and Refrigeration Center. College of Engineering …, 1993.
[49] A. Cavallini, D. Del Col, L. Doretti, M. Matkovic, L. Rossetto, C. Zilio, Condensa-

tion heat transfer and pressure gradient inside multiport minichannels, Heat Transf. Eng. 26 (2005) 45–55.
[50] B. Mitra, Supercritical gas cooling and condensation of refrigerant R410A at near-critical pressures, (2005).
[51] J.S. Shin, M.H. Kim, An experimental study of flow condensation heat transfer inside circular and rectangular mini-channels, in: Int. Conf. Nanochannels, Microchannels, Minichannels, 2004, pp. 633–640.
[52] U.C. Andresen, Supercritical gas cooling and near-critical-pressure condensation of refrigerant blends in microchannels, (2006).
[53] T.M. Bandhauer, A. Agarwal, S. Garimella, Measurement and modeling of condensation heat transfer coefficients in circular microchannels, (2006).
[54] Ö. Ağra, İ. Teke, Experimental investigation of condensation of hydrocarbon refrigerants (R600a) in a horizontal smooth tube, Int. Commun. Heat Mass Transf. 35 (2008) 1165–1171.
[55] Y.J. Kim, J. Jang, P.S. Hrnjak, M.S. Kim, Condensation heat transfer of carbon dioxide inside horizontal smooth and microfin tubes at low temperatures, J. Heat Transf. (2009) 131.
[56] K.A. Maråk, Condensation heat transfer and pressure drop for methane and binary methane fluids in small channels, (2009).
[57] M. Matkovic, A. Cavallini, D. Del Col, L. Rossetto, Experimental study on condensation heat transfer inside a single circular minichannel, Int. J. Heat Mass Transf. 52 (2009) 2311–2323.
[58] C.Y. Park, P. Hrnjak, CO2 flow condensation heat transfer and pressure drop in multi-port microchannels at low temperatures, Int. J. Refrig. 32 (2009) 1129–1139.
[59] M.K. Dobson, Heat transfer and flow regimes during condensation in horizontal tubes, Air Conditioning and Refrigeration Center. College of Engineering…, 1994.
[60] A. Agarwal, T.M. Bandhauer, S. Garimella, Measurement and modeling of condensation heat transfer in non-circular microchannels, Int. J. Refrig. 33 (2010) 1169–1179.
[61] S. Bortolin, Two-phase heat transfer inside minichannels, (2010).
[62] D. Del Col, D. Torresin, A. Cavallini, Heat transfer and pressure drop during condensation of the low GWP refrigerant R1234yf, Int. J. Refrig. 33 (2010) 1307–1318.
[63] X. Huang, G. Ding, H. Hu, Y. Zhu, H. Peng, Y. Gao, B. Deng, Influence of oil on flow condensation heat transfer of R410A inside 4.18 mm and 1.6 mm inner diameter horizontal smooth tubes, Int. J. Refrig. 33 (2010) 158–169.
[64] O. Iqbal, P. Bansal, In-tube condensation heat transfer of CO2 at low temperatures in a horizontal smooth tube, Int. J. Refrig. 35 (2012) 270–277.
[65] H.-K. Oh, C.-H. Son, Condensation heat transfer characteristics of R-22, R-134a and R-410A in a single circular microtube, Exp. Therm. Fluid Sci. 35 (2011) 706–716.
[66] J.E. Park, F. Vakili-Farahani, L. Consolini, J.R. Thome, Experimental study on condensation heat transfer in vertical minichannels for new refrigerant R1234ze (E) versus R134a and R236fa, Exp. Therm. Fluid Sci. 35 (2011) 442–454.
[67] M. Derby, H.J. Lee, Y. Peles, M.K. Jensen, Condensation heat transfer in square, triangular, and semi-circular mini-channels, Int. J. Heat Mass Transf. 55 (2012) 187–197.
[68] M.A. Hossain, Y. Onaka, A. Miyara, Experimental study on condensation heat transfer and pressure drop in horizontal smooth tube for R1234ze (E), R32 and R410A, Int. J. Refrig. 35 (2012) 927–938.
[69] K. Sakamatapan, J. Kaew-On, A.S. Dalkilic, O. Mahian, S. Wongwises, Condensation heat transfer characteristics of R-134a flowing inside the multiport minichannels, Int. J. Heat Mass Transf. 64 (2013) 976–985.
[70] H. Hirofumi, R.L. Webb, Condensation in extruded aluminum tubes, Penn State (1995).
[71] N. Liu, J.M. Li, J. Sun, H.S. Wang, Heat transfer and pressure drop during condensation of R152a in circular and square microchannels, Exp. Therm. Fluid Sci. 47 (2013) 60–67.
[72] J. Heo, H. Park, R. Yun, Condensation heat transfer and pressure drop characteristics of CO2 in a microchannel, Int. J. Refrig. 36 (2013) 1657–1668.
[73] F. Illan-Gomez, A. Lopez-Belchi, J.R. Garcia-Cascales, F. Vera-Garcia, Experimental two-phase heat transfer coefficient and frictional pressure drop inside mini-channels during condensation with R1234yf and R134a, Int. J. Refrig. 51 (2015) 12–23.
[74] G. Ghim, J. Lee, Condensation heat transfer of low GWP ORC working fluids in a horizontal smooth tube, Int. J. Heat Mass Transf. 104 (2017) 718–728.
[75] J. Kaew-On, N. Naphattharanun, R. Binmud, S. Wongwises, Condensation heat transfer characteristics of R134a flowing inside mini circular and flattened tubes, Int. J. Heat Mass Transf. 102 (2016) 86–97.
[76] N. Liu, H. Xiao, J. Li, Experimental investigation of condensation heat transfer and pressure drop of propane, R1234ze (E) and R22 in minichannels, Appl. Therm. Eng. 102 (2016) 63–72.
[77] S.-M. Kim, I. Mudawar, Flow condensation in parallel micro-channels–part 2: heat transfer results and correlation technique, Int. J. Heat Mass Transf. 55 (2012) 984–994.
[78] M. Zhang, A new equivalent Reynolds number model for vapor shear-controlled condensation inside smooth and micro-fin tubes, ProQuest Information and Learning, 1998.
[79] W.-W.W. Wang, Condensation and single-phase heat transfer coefficient and flow regime visualization in microchannel tubes for HFC-134a, (1999).
[80] Y.-Y. Yan, H.-C. Lio, T.-F. Lin, Condensation heat transfer and pressure drop of refrigerant R-134a in a plate heat exchanger, Int. J. Heat Mass Transf. 42 (1999) 993–1006.
[81] J.R. Baird, D.F. Fletcher, B.S. Haynes, Local condensation heat transfer rates in fine passages, Int. J. Heat Mass Transf. 46 (2003) 4453–4466.
[82] N.-H. Kim, J.-P. Cho, J.-O. Kim, B. Youn, Condensation heat transfer of R-22 and R-410A in flat aluminum multi-channel tubes with or without micro-fins, Int. J. Refrig. 26 (2003) 830–839.
[83] J. Jang, P.S. Hrnjak, Condensation of CO2 at low temperatures, Air Conditioning and Refrigeration Center. College of Engineering …, 2004.
[84] F. Pedregosa, G. Varoquaux, A. Gramfort, V. Michel, B. Thirion, O. Grisel, M. Blondel, P. Prettenhofer, R. Weiss, V. Dubourg, Scikit-learn: machine learning in Python, J. Mach. Learn. Res. 12 (2011) 2825–2830.
[85] C.M. Bishop, Neural Networks for Pattern Recognition, Oxford university press, 1995.
[86] A. Prieto, B. Prieto, E.M. Ortigosa, E. Ros, F. Pelayo, J. Ortega, I. Rojas, Neural networks: An overview of early research, current frameworks and new challenges, Neurocomputing 214 (2016) 242–268, doi:10.1016/J.NEUCOM.2016.06.014.
[87] B. Widrow, M.E. Hoff, Adaptive Switching Circuits, Stanford Univ Ca Stanford Electronics Labs, 1960.
[88] T.G. Dietterich, E.B. Kong, Machine learning bias, statistical bias, and statistical variance of decision tree algorithms, Technical report, Department of Computer Science, Oregon State University, 1995.
[89] T.G. Dietterich, An experimental comparison of three methods for constructing ensembles of decision trees: Bagging, boosting, and randomization, Mach. Learn. 40 (2000) 139–157.
[90] Y. Freund, R.E. Schapire, Experiments with a new boosting algorithm, in: Icml, Citeseer (1996) 148–156.
[91] L. Guelman, Gradient boosting trees for auto insurance loss cost modeling and prediction, Expert Syst. Appl. 39 (2012) 3659–3667.
[92] Z. Zhang, G. Mayer, Y. Dauvilliers, G. Plazzi, F. Pizza, R. Fronczek, J. Santamaria, M. Partinen, S. Overeem, R. Peraita-Adrados, Exploring the clinical features of narcolepsy type 1 versus narcolepsy type 2 from European Narcolepsy Network database with machine learning, Sci. Rep. 8 (2018) 1–11.
[93] L. Breiman, Random forests, Mach. Learn. 45 (2001) 5–32.
[94] J.H. Friedman, Greedy function approximation: a gradient boosting machine, Ann. Stat. (2001) 1189–1232.
[95] T. Chen, C. Guestrin, Xgboost: a scalable tree boosting system, in: Proc. 22nd Acm Sigkdd Int. Conf. Knowl. Discov. Data Min., 2016, pp. 785–794.
[96] D. Nielsen, Tree boosting with xgboost-why does xgboost win" every" machine learning competition?, (2016).
[97] J. Brownlee, in: Machine Learning Mastery with Python, Mach. Learn. Mastery Pty Ltd., 2016, pp. 100–120.
[98] J.S. Bergstra, R. Bardenet, Y. Bengio, B. Kégl, Algorithms for hyper-parameter optimization, in: Adv. Neural Inf. Process. Syst., 2011, pp. 2546–2554.
[99] J. Bergstra, Y. Bengio, Random search for hyper-parameter optimization, J. Mach. Learn. Res. 13 (2012) 281–305.
[100] S. Yang, H. Zhang, Comparison of several data mining methods in credit card default prediction, Intell. Inf. Manag. 10 (2018) 115.
[101] M.A. Fauzan, H. Murfi, The accuracy of XGBoost for insurance claim prediction, Int. J. Adv. Soft Comput. Appl. (2018) 10.
[102] H.A. Simon, Spurious correlation: a causal interpretation, J. Am. Stat. Assoc. 49 (1954) 467–479.
[103] H.A. Simon, Spurious correlation: a causal interpretation, in: Model. Discov., Springer, 1977, pp. 93–106.
[104] P. Reasor, V. Aute, R. Radermacher, Refrigerant R1234yf performance comparison investigation, (2010).